①

Doctoral Thesis

Isotope Shift and Hyperfine Structure in Yb I by Atomic-Beam Laser Spectroscopy

Wei–Guo JIN

Department of Physics, Faculty of Science,
Hiroshima University, Higashi-Hiroshima 724, JAPAN

(October, 1991)

Contents

Abstract

Isotope shifts of 9 transitions from the ground and metastable states in Yb I were measured for 7 stable isotopes with A=168–176 by means of atomic-beam laser spectroscopy. The electric discharge was used to obtain the intense population of the metastable state in Yb I. Hyperfine constants A and B of 12 levels for ^{171}Yb and ^{173}Yb were determined. Reliable values of nuclear parameters λ were obtained and changes in mean square nuclear charge radii $\delta\langle r^2\rangle$ were deduced using both the two-parameter model and the numerical analysis. Deformations for Yb stable isotopes and the odd-even staggering effect for odd-N isotopes were discussed. Hyperfine constants A and B were analyzed with the effective operator procedure and the single-electron hyperfine parameters of $6s$ and $6d$ electrons were derived for the Yb I $4f^{14}6s6d$ configuration. For the ^3D_J and $^1D_2$ states of $4f^{14}6s6d$, J and term dependences of isotope shifts were obtained and the parameters of the crossed-second-order effect were derived to be $z_{6d}/\lambda = 18(6)$ MHz/fm^2 and $g_2(6s, 6d)/\lambda = -1120(60)$ MHz/fm^2.

1. Introduction

Isotope shift (IS) is the energy shift of an optical transition between different isotopes for one element. When a neutron is added or taken out from a nucleus, the reduced mass of atomic electron, the correlation between electrons and the charge distribution of the nucleus are changed. This results in the changes of kinetic energy and potential energy of electrons which correspond to the isotope shift. Hyperfine structure (HFS) originates from the magnetic dipole and electric quadrupole interaction between electrons and the nucleus, since the nucleus has a magnetic dipole and electric quadrupole moments. Because isotope shift has an order of magnitude of 10^3 MHz which is comparable to HF splitting of 10^2–10^3 MHz, studies of IS and HFS are always connected.

Measurements of isotope shift and hyperfine structure yield the informations not only for the nucleus but also for the electronic property of the atom. From the isotope shift, the information about the nuclear charge distribution and the nuclear shape can be extracted. The important parameters related to the charge distribution are changes in mean square nuclear charge radii $\delta\langle r^2\rangle$ and deformation parameters $\delta\langle\beta^2\rangle$. From the hyperfine structure, the nuclear spin, the nuclear magnetic dipole moment μ and the nuclear electric quadrupole moment Q are derived. The parameters of the nucleus $\delta\langle r^2\rangle$, μ and Q are the basic ones for the nuclear ground state and comparison of these parameters with theoretical calculations could give insight and information about nuclear structure. The IS and HFS also give out the electronic information such as the radial integral $\langle r^{-3}\rangle$, the electron density at the nucleus, the configuration mixing and the electron screening effect. These effects related to behavior of electrons are of great help to atomic physics. Therefore, study of IS and HFS is a unique way, compared with the nuclear reactions such as electron scattering, inelastic scattering of proton and α-particle and Coulomb excitation, to deepen the understanding of the nucleus and electrons.

Studies of IS and HFS have a long history. The conventional optical spectroscopy (*e.g.* Fabry-Perot interferometer) was widely used in the early days. But obtained values have the uncertainty of several % and less values exist for isotopes with small abundance. Early works of IS and HFS were reviewed by Heilig and Steudel,[1] and

Childs.[2] It was the CW tunable dye laser that revolutionized the optical spectroscopy with its high resolution and high sensitivity[3] from the early 1970. The fluctuation of laser frequency is as small as several MHz and this leads to an energy resolution of $\delta\nu/\nu \leq 10^{-7}$. The power of the dye laser beam reaches to several watts, thus atomic beam can be as small as 10^3atoms/s for laser induced fluorescence measurements. The values of IS and HFS are obtained with the uncertainty of an order of 0.1 % by the laser spectroscopy. Measurements are also possible even for isotopes with very small abundance. Studies across long isotopic chain are possible for stable and unstable isotopes by this technique and this is particularly superior to other methods for nuclear study, for example, nuclear reaction and Coulomb excitation *etc.*, where enriched isotope target is always necessary. Studies of IS and HFS for the stable and unstable[4,5] nuclei have been extensively done by the laser spectroscopy in recent years and were recently reviewed by Otten.[6] Particularly, many works[7–16] have been carried out for the stable isotopes of the rare-earth elements by the atomic-beam laser spectroscopy because the beam of the stable isotopes is easily obtained. Very reliable informations can be extracted for stable isotopes. To get the information about the electronic property, the atomic-beam laser spectroscopy is usually used.

The nuclear parameters $\delta\langle r^2\rangle$ and $\delta\langle\beta^2\rangle$ are extracted from the isotope shift. The general trends of $\delta\langle r^2\rangle$ were already known for most of stable isotopes by the conventional optical spectroscopy,[1] but the uncertainty is more than 10 %. Since values of $\delta\langle r^2\rangle$ can be evaluated by using, for example, the liquid-drop or droplet model, more precise values of $\delta\langle r^2\rangle$ are needed to check these nuclear models. The nuclear deformation has been found to be mainly quadrupole and higher order deformations have been understood very little. The deformation parameter $\delta\langle\beta^2\rangle$ deduced from IS is contributed from not only quadrupole but also higher order deformations. Thus, informations about nuclear quadrupole and higher order deformations can be obtained from IS. Recently, strong octupole deformation was found for Ra isotopes from IS measurements.[4]

From HFS, one can determine HF coupling constants A and B which describe the magnetic dipole and electric quadrupole interactions, respectively. Hyperfine constants A and B were reported for the ground state and some low-lying levels.[17] Recently, precise values of A and B have been determined for high-energy levels of some rare-earth elements by the laser spectroscopy.[10,18] HF constants A and B are contributed from each electron of open atomic shells. To study the behavior and contribution of a single electron for the HF interaction, the single-electron HF parameter is introduced. The effective operator procedure[19] is used to extract the single-electron hyperfine parameters from the measured values of A and B. Such studies were well reported for $4f$, $5d$, $6s$ and $6p$ electrons of the rare-earth elements and recently reviewed by Pfeufer.[20]

Isotope shift mainly depends on the electronic configuration and should be dependent on electronic term and angular momentum J just like the atomic level energy. In 1976, Bauche and Champeau[21] attributed term and J dependences of IS to the so-called crossed-second-order (CSO) effect of IS and refined parametric description of the CSO effect. The CSO effect is the effect of configuration mixing from very-far atomic levels. The effect of the configuration mixing is very important one for theoretical calculations and is actually related to the behavior of the electron. Particularly, it is only the CSO effect which can give information about the mixing effect from very far configurations. Investigations of the CSO effect were reported for some configurations of low-energy levels for $4f$ and $5d$ electrons of the rare-earth elements.[16,22–25]

Ytterbium with the atomic number Z=70 is the last even-Z element in the rare-earth region and has closed $4f$ and $6s$ subshells in the ground state. The ground configuration $4f^{14}6s^2$ only yields one state $^1S_0$ (the ground state). Atomic spectrum shows an alkaline-earth like character when $4f$-shell is not broken and also becomes complicated when $4f$ electrons are excited. Because there are no other states ($<10^4$ cm^{-1}) near the ground state which are thermally populated, less transitions exist in the visible wavelength region of the dye laser and reported studies of IS and HFS are less. From the standpoint of nuclear side, stable isotopes of Yb have the neutron number N=98–106 and lie almost in the middle of two closed shells (N=82 and 126). For Yb stable isotopes, Clark *et al.*[13] measured isotope shifts of one transition by the atomic-beam laser spectroscopy and derived nuclear parameters λ related to $\delta<r^2>$ by combining the optical IS with the electronic and muonic X-ray IS's. However, such analysis seems to have some ambiguities because the definition of the nuclear parameter of optical IS differs slightly from that of the muonic X-ray IS. Baumann and Braun[26] measured HF constants A and B for the $4f^{14}6s6d\ ^3D_J$ and $^1D_2$ states of ^{171}Yb and ^{173}Yb by means of two-step laser excitation, but the results have large uncertainties. Moreover, single-electron HF parameters for $6d$ electron are not reported. Concerning the CSO effect, no report can be found for the $6d$ electron of Yb.

We have measured IS and HFS for the stable isotopes[14–16] of Nd, Sm, Gd, Dy and Er. The nuclear deformation has been examined for the nuclei with the neutron mumber N=82–102. To study the nuclear deformation of Yb and extend our systematic study up to N=106, we carry out measurements of IS and HFS in Yb I. Another purpose of this study is to measure IS and HFS for excited upper configurations and to investigate the HF interaction and the CSO effect for the $6d$ electron. For the study of upper levels, transitions from metastable states are chosen and an electric discharge is used to populate metastable states. This thesis will describe details about experimental setup of laser spectroscopy and method of electric discharge as well as methods of analysis for IS and HFS. We try to extract reliable values of $\delta\langle r^2\rangle$ for the stable isotopes of Yb by means of atomic-beam laser spectroscopy and to examine the deformation of these isotopes. We can obtain HF constants A and B, and term and J dependences of IS. Moreover, single-electron HF parameters and CSO parameters can be determined for $6s$ and $6d$ electrons. Discussion about experimental results will be also given.

2. Experimental

2.1 Experimental setup

The experimental setup is shown schematically in Fig. 1. An Ar-ion laser (Spectra-physics 2016) with 5-W power was used to pump a ring dye laser (Spectra-physics 380A) which gives out the continuously tunable laser light. Dyes of Rhodamine 6G and 110 were used and a wavelength range of about 530–610 nm was available. The typical power of the dye laser was about 100 mW during the experiment and the fluctuation of the frequency was about 5 MHz. The continuous scanning of the laser frequency over 30 GHz was available.

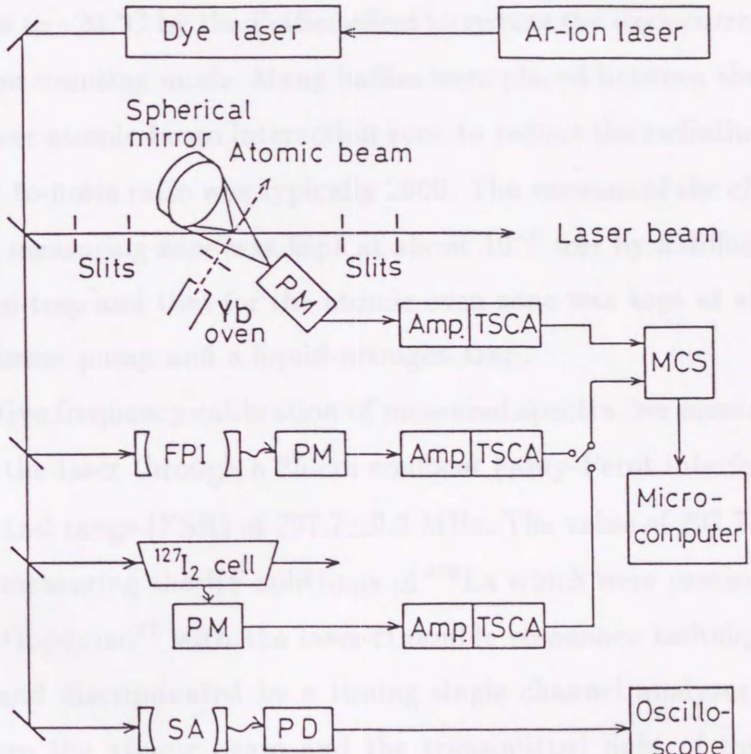

Fig. 1. General layout of the experimental setup. Abbreviations are as follows: PM: photomultiplier. Amp.: amplifier. TSCA: timing single channel analyzer. FPI: Fabry-Perot interferometer. SA: spectrum analyzer. PD: photodiode. MCS: multi-channel scaler.

The laser beam was collimated by four slits of 3 mm in diameter in the vertical direction. The atomic beam was ejected from a small hole (0.5 mm in diameter) of the oven and collimated with a second slit of 2 mm in diameter at a distance of 20 cm from the oven in the horizotal direction. The collimation ratio is 100 and this means that the loss of atomic beam is about 10^4 by the second slit. The laser beam was crossed orthogonally with the atomic beam and the Doppler broadening was greatly reduced. The residual Doppler broadening is about 10 MHz. Increase of the collimation ratio would reduce the Doppler broadening but yield larger loss of the atomic beam. The resonant fluorescence from the atomic beam, induced by the laser beam, was focussed by a spherical mirror and was detected by a photomultiplier (PM). The solid angle for the photon detection was enlarged to 1.4π sr by the spherical mirror with a diameter of 8 cm and a radius of curvature of 6 cm. The photomultiplier (Hamamatsu 643-02) was cooled down to -20 °C by the Peltier effect to reduce the dark current and used in the single photon counting mode. Many baffles were placed between the atomic beam oven and the laser atomic-beam interaction zone to reduce the radiation background. Then the signal-to-noise ratio was typically 2000. The vacuum of the chamber for the interaction and measuring zone was kept at about 10^{-6} torr by a diffusion pump and a liquid-nitrogen trap and that for the atomic oven zone was kept at about 10^{-5} torr by another diffusion pump and a liquid-nitrogen trap.

For the relative frequency calibration of measured spectra, we measured the transmitted light of the laser through a 25-cm confocal Fabry-Perot interferometer (FPI) with a free spectral range (FSR) of 297.7±0.2 MHz. The value of 297.7±0.2 MHz was determined by measuring the HF splittings of ^{139}La which were precisely determined by Childs and Goodman[27] with the laser-rf double resonance technique. The signal was amplified and discriminated by a timing single channel analyzer (TSCA). The fluorescence from the atomic beam and the transimitted light of the FPI were simultaneously recorded with a dual-input multichannel scaler (MCS). The MCS with 32768×2 channel memories was controlled by a microcomputer and worked with 50 channels per second. The scanning speed of the laser was about 100 MHz per second and the data taking time for one spectrum was about 3 min. The absolute wave number of the transition was determined by measuring the emission spectra of an $^{127}I_2$

cell since the rotational spectra of $^{127}I_2$ molecule were already well measured.[28] The transmitted light through a spectrum analyzer (SA) with FSR of 2 GHz was detected by a photodiode (PD) and the frequency scanning of the dye laser was monitored with the oscilloscope.

2.2 Population of the metastable state in Yb I by means of an electric discharge

Populations of various states in the atomic beam are given by the Boltzman distribution. Only low-lying levels are thermally populated for the temperature below 2000 °C. To study the transitions from upper-lying metastable states, populations of such metastable states are necessary. Electric discharge is a convenient and unique method to populate metastable states and has been used[8,9,29] for Ba, Sm and Eu, etc. However, details of processes to populate metastable states are not known to us and no reports have been found for Yb in the literature. For studies of IS and HFS of the metastable states and higher excited levels of Yb I, we constructed an atomic beam oven of a discharge type. Details on the population of metastable states of Yb I by electric discharge were examined.[30]

Figure 2 shows the atomic beam oven of a discharge type. A molybdenum crucible (8 mm in diameter and 20 mm in length) loaded with Yb (about 0.3 g) is mounted

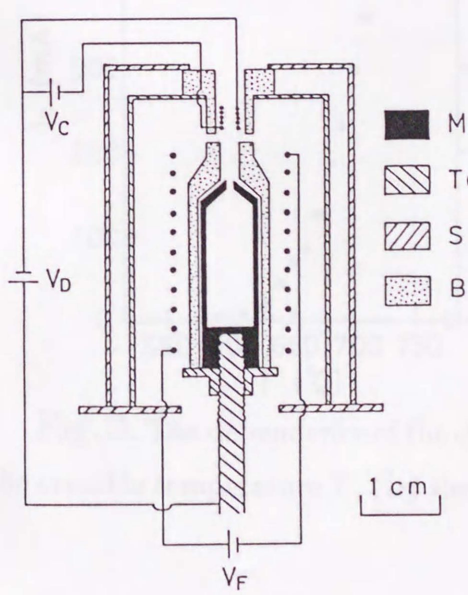

Fig. 2. Atomic beam oven of the discharge type. V_F: voltage of the crucible filament, V_C: cathode heating voltage, V_D: discharge voltage. ST and BN are the abbreviations of stainless steel and boron nitride, respectively.

on top of a tantalum rod. An atomic beam of Yb is ejected from a small orifice with a diameter of 0.5 mm by means of resistance heating of a crucible filament. Boron nitride (BN) is used as insulators. The oven temperature up to 2000 °C is easily obtained with the help of tantalum and stainless steel heat shields. The temperature T of the crucible is measured by a Pt-Rh thermocouple. The discharge cathode is a Ta wire of 0.5 mm in diameter in a 5-turn helical coil of 3 mm in diameter, 4 mm in length and is placed at about 7 mm from the crucible in the beam direction. The crucible itself serves as a discharge anode, and electric discharge is produced around the orifice of the crucible.

The dependence of the discharge current I_D on the crucible temperature T, on the cathode current I_C and on the discharge voltage V_D is shown in Fig. 3. Figure 3 (a) shows that the discharge current is very small at the crucible temperature of 600 °C and drastically increases when the crucible temperature reaches 700 °C (corresponding to the vapor pressure of about 2.5 torr). Temperature above 700 °C is not necessary because the discharge becomes unstable above 700 °C. Stable discharge is easily attained at the cathode heating current of 7 A, as shown in Fig. 3 (b). Higher

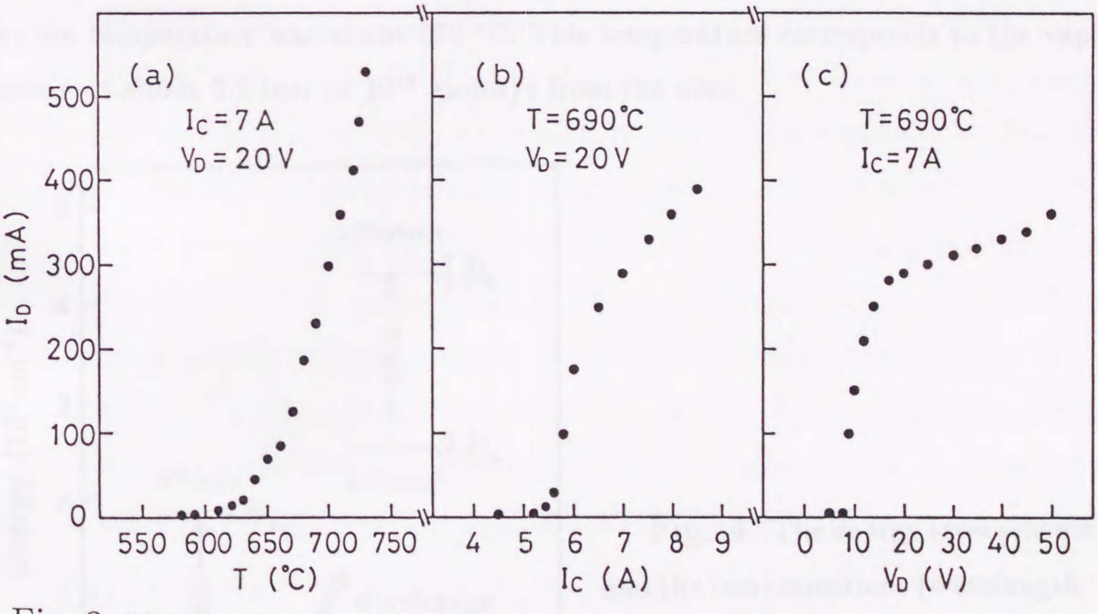

Fig. 3. The dependence of the discharge current I_D on the various parameters: (a) the crucible temperature T, (b) the cathode current I_C, (c) the discharge voltage V_D.

cathode-heating current caused the discharge at lower temperature but produced strong background for the laser-induced fluorescence measurements. The cathode with the heating current of up to 7 A yielded almost no such background. Figure 3 (c) shows that the discharge current is not very sensitive to the discharge voltage in the range of 15–50 V. A discharge voltage over 50 V is too high and causes the discharge to become unstable. Thus, it was found that the conditions to maintain the stable discharge are 650–700 °C for the crucible temperature, about 7 A for the cathode current and 20–50 V for the discharge voltage.

The relative population of the metastable state of Yb I was studied by measuring laser-induced fluorescence of two optical transitions. The simplified energy level scheme[31] and the studied transitions are shown in Fig. 4. The 555.65 nm transition is from the $^1S_0$ ground state of the $4f^{14}6s^2$ configuration to the 17992 cm^{-1} $^3P_1$ state of the $4f^{14}6s6p$ configuration. Since the ground state of Yb I is $^1S_0$, the 25860 cm^{-1} $(7/2,3/2)_5$ (expression of jj coupling scheme: $(j_1, j_2)_J$) state of the $4f^{13}5d6s^2$ configuration is a metastable state. The 585.45 nm transition is from this metastable state to the 42936 cm^{-1} $(7/2,3/2)_5$ state of the $4f^{13}5d6s6p$ configuration. For the measurement of the 555.65 nm transition from the ground state, no discharge was needed and the oven temperature was about 570 °C. This temperature corresponds to the vapor pressure of about 0.2 torr or 10^{14} atoms/s from the oven.

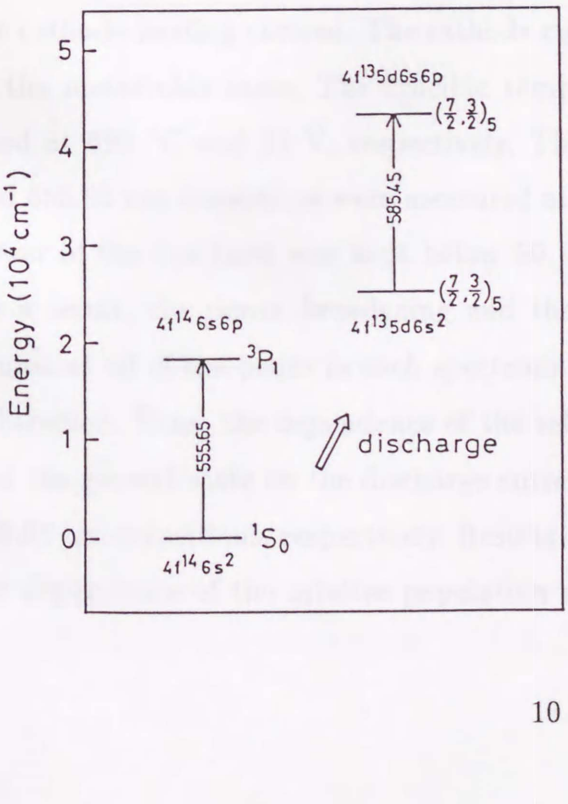

Fig. 4. The energy level scheme and the two transitions (wavelength in nm) in Yb I to measure the population of the metastable state by the electric discharge.

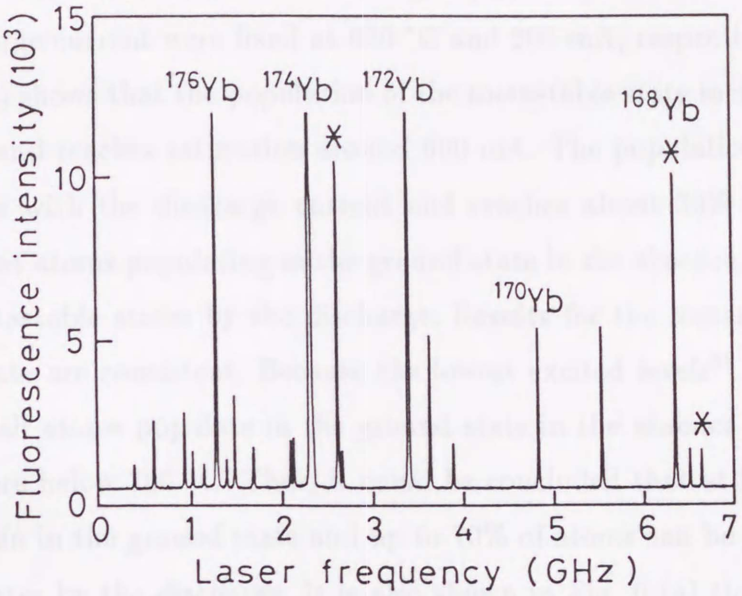

Fig. 5. The laser-induced fluorescence spectrum of the 585.45 nm transition. The peaks of even-mass isotopes are labelled with the isotope symbol. Peaks marked with (*) are the hyperfine peaks of ^{171}Yb and other peaks are the hyperfine peaks of ^{173}Yb.

The measured fluorescence spectrum of the 585.45 nm transition is shown in Fig. 5. Not only the peaks of even-mass isotopes of $^{168-176}$Yb but the HF peaks of ^{171}Yb (nuclear spin I=1/2) and ^{173}Yb (I=5/2) are well resolved, except the accidental overlap of ^{168}Yb and one HF peak of ^{171}Yb. The discharge current was controlled by changing the cathode heating current. The cathode current had no influence on the population of the metastable state. The crucible temperature and the discharge voltage were fixed at 690 °C and 23 V, respectively. The fluorescence spectra of the 585.45 nm and 555.65 nm transitions were measured at different discharge currents. The output power of the dye laser was kept below 50 μW by means of a neutral density filter. As a result, the power broadening and the saturation effects were negligible. The counts at all of the peaks in each spectrum were integrated and the background was subtracted. Thus, the dependence of the relative population of the metastable state and the ground state on the discharge current was obtained from the 585.45 nm and 555.65 nm transitions, respectively. Results are shown in Fig. 6 (a). In the same way, the dependence of the relative population of the metastable state on the discharge voltage was also obtained and is shown in Fig. 6 (b), where the crucible temperature and the discharge current were fixed at 690 °C and 200 mA, respectively.

Figure 6 (a) shows that the population of the metastable state increases gradually until 300 mA and reaches saturation around 600 mA. The population of the ground state decreases with the discharge current and reaches about 30% above 500 mA. This means that atoms populating in the ground state in the absence of discharge are excited to metastable states by the discharge. Results for the metastable state and the ground state are consistent. Because the lowest excited levels[31] lie above 17000 cm^{-1}, almost all atoms populate in the ground state in the absence of discharge for the temperature below 700 °C. Thus, it could be concluded that at least about 30% of atoms remain in the ground state and up to 70% of atoms can be populated in all metastable states by the discharge. It is also shown in Fig. 6 (a) that the discharge current of 200–400 mA is best and can produce a relative population of 60–90% of the metastable state. Figure 6 (b) shows that the population of the metastable state is less sensitive to the discharge voltage in the range of 20–50 V.

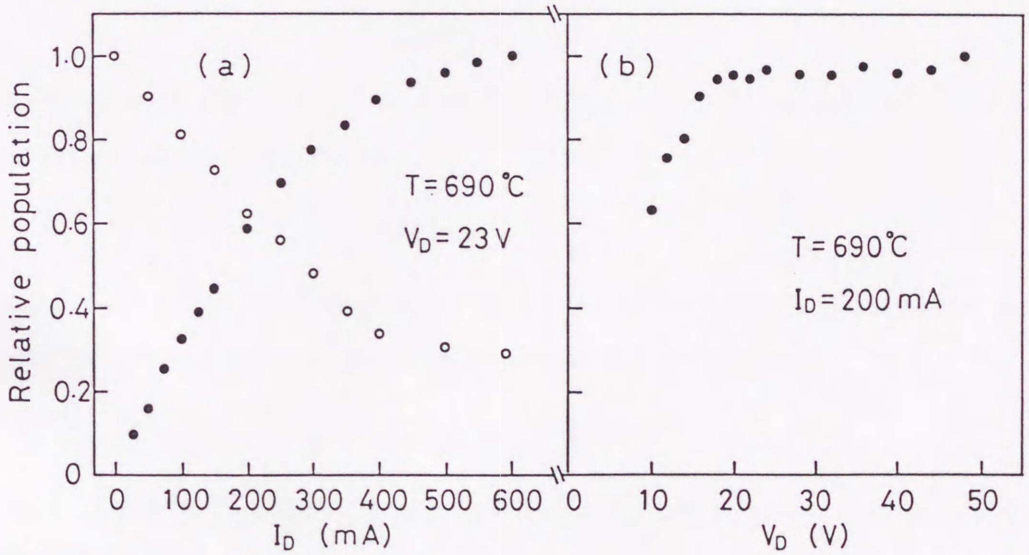

Fig. 6. (a) The dependence of the relative population of the $(7/2,3/2)_5$ state of $4f^{13}5d6s^2$ (closed circles) and the ground state (open circles) on the discharge current I_D. Normalizations were carried out at a discharge current of 600 mA for the metastable state and at the absence of the discharge for the ground state. (b) The dependence of the relative population of the metastable state on the discharge voltage V_D. Normalization was carried out at a discharge voltage of 50 V.

In summary, the best conditions to obtain intense population in the metastable states are as follows: 650–700 °C for the crucible temperature, above 7 A for the cathode current, 20–50 V for the discharge voltage and 200–400 mA for the discharge current. The population of the metastable state of Yb I strongly depends on the discharge current and is less sensitive to the discharge voltage above 20 V. The population of all metastable states up to about 70% can be obtained by the discharge. This method can also be applied for the laser spectroscopy of metastable states of other elements.

3. Theoretical Description

3.1 Isotope shift

The observed isotope shift $\delta\nu_i$, between isotopes with mass number A and A' for a transition i, is the sum of the normal mass shift (NMS), the specific mass shift (SMS) and the field shift (FS). Then $\delta\nu_i$ can be written as[1],

$$\delta\nu_i = \delta\nu_{i\mathrm{NMS}} + \delta\nu_{i\mathrm{SMS}} + \delta\nu_{i\mathrm{FS}}, \tag{1}$$

where the normal mass shift (NMS) $\delta\nu_{i\mathrm{NMS}}$ is caused by the change in the reduced mass of electron and nucleus and is calculated easily. The specific mass shift (SMS) $\delta\nu_{i\mathrm{SMS}}$ is caused by the correlation between electrons, and its calculation is very difficult particularly for rare-earth elements and yields only qualitative agreement with experimental results.

$$\delta\nu_{i\mathrm{NMS}} = M_{i\mathrm{NMS}} \frac{A' - A}{AA'}, \tag{2}$$

$$\delta\nu_{i\mathrm{SMS}} = M_{i\mathrm{SMS}} \frac{A' - A}{AA'}, \tag{3}$$

where $M_{i\mathrm{NMS}}$ and $M_{i\mathrm{SMS}}$ are the factors of NMS and SMS, respectively. The factor $M_{i\mathrm{NMS}}$ has the simple expression,

$$M_{i\mathrm{NMS}} = \frac{\nu_i}{1836.15}, \tag{4}$$

where ν_i is the transition frequency. For a pure $ns^2 - nsnp$ transition, the SMS is negligibly small and the semiempirical evaluation is usually used,

$$\delta\nu_{\mathrm{SMS}} = (0 \pm 0.5)\delta\nu_{\mathrm{NMS}}. \tag{5}$$

The field shift (FS) $\delta\nu_{i\mathrm{FS}}$ is caused by the change in the nuclear charge distribution and is given in first-order perturbation theory by

$$\delta\nu_{i\mathrm{FS}} = F_i\lambda = E_i f(Z)\lambda, \tag{6}$$

where the nuclear parameter λ is related to the change in mean square nuclear charge radii $\delta{<}r^2{>}$ and higher order contributions.

$$\lambda = \sum_n \frac{C_n}{C_1}\delta < r^{2n} >= \delta < r^2 > + \frac{C_2}{C_1}\delta < r^4 > + \frac{C_3}{C_1}\delta < r^6 > + \cdots, \tag{7}$$

where the expansion coefficients C_1, C_2 and C_3 are calculated by Seltzer.[32] The relativistic correction factor $f(Z)$ of the FS depends on the atomic number Z and is given by Ahmad *et al.*[4] as follows,

$$f(Z) = \frac{C_{\text{unif}}}{\sum_n \frac{C_n}{C_1} \frac{2n}{2n+3} r_0^{2n} \bar{A}^{-\frac{2n}{3}-1}(A' - A)}, \tag{8}$$

where $\bar{A} = \frac{1}{2}(A + A')$ and r_0=1.2 fm. The isotope shift constant C_{unif} is recalculated recently by Blundell *et al.*[33] for the nucleus of a uniformly charged sphere. Equation (8) differs from the conventional definition of $f(Z)$ in ref. 1 because the higher order contributions of $\delta\langle r^4\rangle$ and $\delta\langle r^6\rangle$ were omitted in ref. 1

The electronic factor E_i is related to the change of the nonrelativistic electron charge density $\delta \mid \psi(0) \mid_i^2$ at the nucleus,

$$E_i = \pi a_0^3 \delta \mid \psi(0) \mid_i^2 /Z, \tag{9}$$

where a_0 is the Bohr radius. According to the semiempirical evaluation,[1] $\delta \mid \psi(0) \mid_i^2$ can be determined from the charge density $\mid \psi(0) \mid_{ns}^2$ of the s electron,

$$\delta \mid \psi(0) \mid_{ns-np}^2 = \beta \mid \psi(0) \mid_{ns}^2, \tag{10}$$

$$\delta \mid \psi(0) \mid_{ns^2-nsnp}^2 = \gamma \mid \psi(0) \mid_{ns}^2, \tag{11}$$

where β and γ are the screening factors and values of β=1.12 and γ=0.73 were estimated for the rare-earth elements.[1] Thus, E_{ns^2-nsnp} is written as

$$E_{ns^2-nsnp} = \gamma E(ns), \tag{12}$$

with the definition of $E(ns)$,

$$E(ns) = \pi a_0^3 \mid \psi(0) \mid_{ns}^2 /Z. \tag{13}$$

The electron density $\mid \psi(0) \mid_{ns}^2$ of the s electron can be determined empirically for an alkalilike atom. This can be done from the fine structure level scheme by the Goudsmit-Fermi-Segrè formula,[6]

$$\mid \psi(0) \mid_{ns}^2 = \frac{Z Z_a^2}{\pi a_0^3 n_a^3} \frac{dn_a}{dn}, \tag{14}$$

where n_a and dn_a/dn are the effective quantum number of the ns electron and its derivative, respectively. Z_a is the outer charge and is taken to be 1 for neutral atoms, 2 for singly ionized atoms, *etc.* $|\psi(0)|^2_{ns}$ is also determined from the Fermi-contact parameter a_{ns} of the hyperfine structure,[6]

$$|\psi(0)|^2_{ns}= \frac{a_{ns}}{\frac{4}{3}\mu_{\mathrm{B}}\mu_{\mathrm{N}}(\mu/I)F_r(Z)(1-\delta)(1-\varepsilon)}, \tag{15}$$

where μ_{B} and μ_{N} are the Bohr and nuclear magnetons, respectively. I is the nuclear spin and μ is the nuclear magnetic dipole moment. $F_r(Z)$ is the relativistic correction factor. $(1-\delta)$ and $(1-\varepsilon)$ are the Breit-Crawford-Schawlow and the Bohr-Weisskopf correction factors, respectively.

3.2 Changes in mean square nuclear charge radii $\delta<r^2>$ and nuclear deformation parameters $\delta<\beta^2>$

A. Two-parameter model

The nuclear parameter λ can be derived from the field shift. The calculations of the higher order terms $\delta<r^4>$ and $\delta<r^6>$ are necessary to obtain changes in mean square nuclear charge radii $\delta<r^2>$ from λ. Such calculation can be done by using the two-parameter model which was proposed by Ahmad *et al.*[4] In this model, the term of $\delta<r^{2n}>$ is divided into spherical and deformation parts,

$$\delta < r^{2n} >= \delta < r^{2n} >_{\mathrm{sph}} +\delta < r^{2n} >_{\mathrm{def}}, \tag{16}$$

with the assumption of a uniform charge distribution with a sharp cutoff at the nuclear surface. The following relation was deduced,

$$\delta < r^{2n} >= \frac{5n}{2n+3}R_1^{2n-2}\delta < r^2 >_{\mathrm{sph}} +\frac{3n}{4\pi}R_1^{2n}\delta < \beta^2 >, \tag{17}$$

where $R_1^2 = \frac{5}{3} <r^2>_{\mathrm{sph}}$. Values of $<r^2>_{\mathrm{sph}}$ and $\delta<r^2>_{\mathrm{sph}}$ for a spherical nucleus can be calculated by using a droplet model.[34] For n=1, equation (17) reads

$$\delta < r^2 >= \delta < r^2 >_{\mathrm{sph}} +\frac{5}{4\pi} < r^2 >_{\mathrm{sph}}\ \delta < \beta^2 > . \tag{18}$$

Equation (18) has been used for many years in the nuclear spectroscopy. By using eq. (17), values of $\delta<r^2>$ and $\delta<\beta^2>$ are related to the value of λ as follows:

$$\delta < r^2 > \; = \; \frac{\lambda - (x-y)\delta < r^2 >_{\mathrm{sph}}}{1+y}, \tag{19}$$

$$\delta < \beta^2 > = \frac{\lambda - (1+x)\delta < r^2 >_{\mathrm{sph}}}{\frac{5}{4\pi}(1+y) < r^2 >_{\mathrm{sph}}}, \tag{20}$$

$$x \; = \; \frac{10C_2}{7C_1}R_1^2 + \frac{5C_3}{3C_1}R_1^4, \tag{21}$$

$$y \; = \; 2\frac{C_2}{C_1}R_1^2 + 3\frac{C_3}{C_1}R_1^4. \tag{22}$$

B. Numerical analysis

Recently, Wakasugi *et al.*[14] proposed a direct numerical analysis of $\delta<r^2>$ instead of the two-parameter model. In such numerical analysis, the Fermi charge distribution with parameters of the nuclear deformation β, the diffuseness s and the hollow depth w is assumed,

$$\rho(r,\theta) = \rho_0 \frac{1 + w(\frac{r}{R(\theta)})^2}{1 + exp(\frac{r-R(\theta)}{t})}, \tag{23}$$

for the well deformed nucleus. The constant ρ_0 is the charge density at the nuclear center, t is related to the diffuseness parameter s as $t=s/4\ln 3$. $R(\theta)$ is written as

$$R(\theta) = R_2(1 + \beta Y_{20}), \tag{24}$$

$$R_2 = R_0/(1 + \frac{\beta^2}{4\pi}), \tag{25}$$

where $R_0=r_0A^{\frac{1}{3}}$ and Y_{20} is the spherical harmonics. Thus, the term $\delta<r^{2n}>$ is calculated by using the following relation,

$$\delta < r^{2n} >= \frac{\int \delta\rho(r,\theta)r^{2n}dV}{\int \rho(r,\theta)dV}. \tag{26}$$

The reduced gamma transition probability $B(E2)$ is related to the charge distribution,

$$B(E2) =\mid \int \rho(r,\theta)r^2 Y_{20}dV \mid^2 . \tag{27}$$

The general trends of the parameters s and w were examined in ref. 14 and the values of $\delta w(A, A-2)$=0.02 between two isotopes with mass numbers of A and A–2 were found to be a good approximation within one element for the rare-earth region. Therefore, the parameters β and s of the charge distribution can be determined by using the nuclear parameter λ from IS and the $B(E2)$ value from Coulomb excitation measurements. Values of $\delta<r^{2n}>$ are derived by using eq. (26) and not only $\delta<r^2>$ values but also $\delta<r^4>$ and $\delta<r^6>$ values can be deduced. This numerical analysis seems to be more realistic than the two-parameter model because the assumption of a uniform charge distribution is not used in this numerical analysis.

3.3 Hyperfine interaction

The hyperfine interaction is usually treated by the effective operator procedure. The Hamiltonian for the interaction is expressed by[19,35,36]

$$H_{\mathrm{HFS}} = \sum_{K=1}^{\infty} T^K(e) \cdot T^K(n), \tag{28}$$

where $T^K(e)$ and $T^K(n)$ are the tensor operators for the electronic and nuclear parts, respectively. The HF interaction energy E_{HFS} is written as

$$\begin{aligned} E_{\mathrm{HFS}} &= <IJF|H_{\mathrm{HFS}}|IJF> \\ &= \sum_{K=1}^{\infty} (-1)^{I+J+F} \left\{ \begin{array}{ccc} I & J & F \\ J & I & K \end{array} \right\} <J||T^K(e)||J><I||T^K(n)||I>, \end{aligned} \tag{29}$$

where J is the electronic angular momentum and $\mathbf{F} = \mathbf{I} + \mathbf{J}$ is the total angular momentum of the atom. It is enough only to consider the magnetic dipole and electric quadrupole interactions for the hyperfine interaction. That makes the summation limit to K=2. By using the Wigner-Eckart theorem,[37] the reduced matrix element $<I||T^K(n)||I>$ is related to the matrix element $<II|T^K(n)|II>$. Since we have $<II|T^1(n)|II>= \mu$ and $<II|T^2(n)|II>= \frac{1}{2}eQ$, E_{HFS} is expressed as

$$E_{\mathrm{HFS}} = \frac{1}{2}C\mathrm{A} + \frac{3C(C+1) - 4I(I+1)J(J+1)}{4I(2I-1)2J(2J-1)}\mathrm{B}, \tag{30}$$

where

$$C = F(F+1) - I(I+1) - J(J+1).$$

The constants A and B are the nuclear magnetic dipole and the electric quadrupole coupling constants, respectively,[38]

$$A = \frac{\mu}{I}[J(J+1)(2J+1)]^{-\frac{1}{2}} < J||T^1(e)||J >, \tag{31}$$

$$B = 2eQ[\frac{2J(2J-1)}{(2J+3)(2J+2)(2J+1)}]^{\frac{1}{2}} < J||T^2(e)||J > . \tag{32}$$

The relativistic description is necessary to describe exactly the hyperfine interaction which is treated by using the effective operators $T^1(e)$ and $T^2(e)$.[19]

$$T^1(e) = 2\mu_B\mu_N\sum_{i=1}^{N}[\mathbf{l}_i < r_i^{-3} >^{01} -\sqrt{10}(\mathbf{s}_i \times \mathbf{C}_i^2)^1 < r_i^{-3} >^{12} +\mathbf{s}_i < r_i^{-3} >^{10}], \tag{33}$$

$$T^2(e) = e\sum_{i=1}^{N}\{-\mathbf{C}_i^2 < r_i^{-3} >^{02} +[\mathbf{s}_i \times (\mathbf{C}_i^4 \times \mathbf{l}_i^3)]^2 < r_i^{-3} >^{13} +(\mathbf{s}_i \times \mathbf{l}_i)^2 < r_i^{-3} >^{11}\}, \tag{34}$$

where $\mathbf{l}$ and $\mathbf{s}$ are the electron orbit and spin operators, respectively. $\mathbf{C}^2$ is the operator of second vector spherical harmonics. $<r^{-3}>_{nl}^{k_s k_l}$ is the effective (relativistic) radial integrals, where k_s and k_l are the ranks of the tensor operator $T^K(e)$ in the spin space and in the orbital space, respectively, and nl means the electron orbit. Since calculations of them are difficult, $<r^{-3}>_{nl}^{k_s k_l}$ are usually treated as free parameters,

$$a_{nl}^{k_s k_l} = 2\mu_B\mu_N\frac{\mu}{I} < r^{-3} >_{nl}^{k_s k_l}, \tag{35}$$

$$b_{nl}^{k_s k_l} = eQ < r^{-3} >_{nl}^{k_s k_l}, \tag{36}$$

$a_{nl}^{k_s k_l}$ and $b_{nl}^{k_s k_l}$ are the single-electron hyperfine parameters to describe the HF constants A and B, respectively. Three parameters of a_{nl}^{01}, a_{nl}^{12}, a_{nl}^{10} for the constant A and three parameters of b_{nl}^{02}, b_{nl}^{13}, b_{nl}^{11} for the constant B are introduced for each open electron shell nl. Thus, hyperfine constants A and B are written as[20]

$$A = \sum_{nl}\{\alpha_{nl}^{01}(J)a_{nl}^{01} + \alpha_{nl}^{12}(J)a_{nl}^{12} + \alpha_{nl}^{10}(J)a_{nl}^{10}\}, \tag{37}$$

$$B = \sum_{nl}\{\beta_{nl}^{02}(J)b_{nl}^{02} + \beta_{nl}^{13}(J)b_{nl}^{13} + \beta_{nl}^{11}(J)b_{nl}^{11}\}, \tag{38}$$

where summation ranges over all open electron shells in the relevant configuration. $\alpha_{nl}^{k_s k_l}(J)$ and $\beta_{nl}^{k_s k_l}(J)$ are the angular coefficients and depend on J. Calculations of $\alpha_{nl}^{k_s k_l}$ and $\beta_{nl}^{k_s k_l}$ need the state wavefunction (intermediate-coupling wavefunction) which is a linear combination of the pure LS coupling state,

$$|J>=\sum_{LS}\alpha_i|LSJ>_{LS}, \tag{39}$$

where α_i is the coefficient of the intermediate-coupling wavefunction. Equations to calculate $\alpha_{nl}^{k_s k_l}$ and $\beta_{nl}^{k_s k_l}$ for the pure LS coupling state $|LSJ>_{LS}$ have been given by Childs for two-[39] and three-electron[10] shells.

3.4 Crossed-second-order (CSO) effect

In the first-order perturbation theory, the isotope shift depends only on the electronic configuration. J and term dependences of IS result from the crossed-second-order effect which is also called the far-configuration-mixing effect. The mixings from the close-lying levels are treated in the intermediate-coupling wavefunction and mixings from much higher states are taken into consideration in the crossed-second-order effect.

The crossed-second-order contribution to the isotope shift of the pure configuration state with the zeroth-order wavefunction ψ_0 and the energy E_0 is given by Bauche and Champeau,[21] and is written as follows:

$$E_{\mathrm{CSO}}=2\sum_x\frac{<\psi_0|\hat{\mathrm{Q}}|\psi_x><\psi_x|\hat{\mathrm{O}}|\psi_0>}{E_0-E_x}, \tag{40}$$

where ψ_x and E_x are the zeroth-order wavefunctions and the energies of other configurations, respectively. The sum ranges over all states x of all other electronic configurations. $\hat{\mathrm{Q}}$ denotes the operator of the electrostatic interaction or the magnetic interaction of all electrons. $\hat{\mathrm{Q}}$ is expressed by

$$\hat{\mathrm{Q}}=\sum_{i>j}\frac{e^2}{r_{ij}}, \tag{41}$$

for the electrostatic interaction;

$$\hat{\mathrm{Q}}=\sum_i\zeta_i\mathbf{l}_i\cdot\mathbf{s}_i, \tag{42}$$

for the spin-orbit interaction which is the main contribution in the magnetic interaction. ζ_{nl} is the spin-orbit radial integral. $\hat{\mathrm{O}}$ denotes the IS operator,

$$\hat{\mathrm{O}} = \frac{1}{2M}\sum_i P_i^2, \tag{43}$$

for the normal mass shift, where P_i is the momentum of the electron and M is the nuclear mass.

$$\hat{\mathrm{O}} = \frac{1}{M}\sum_{i>j} P_i \cdot P_j, \tag{44}$$

for the specific mass shift.

$$\hat{\mathrm{O}} = C_M \sum_i \delta(r_i), \tag{45}$$

for the field shift, where C_M is a nuclear-dependent part. For the field shift, the configuration which contributes to the field shift in eq. (40) is only that of the $n's$ shell which is excited from the core ns shell.

The CSO contribution between the eletrostatic operator and the isotope shift operator leads to the term dependence of IS in a pure configuration. The term dependence of IS is described by the parameter g_k with the angular coefficient c_k which is the same as that of the electrostatic exchange integral (Slater integral)[40,41] G_k. Whereas the CSO contribution between the magnetic operator and the isotope shift operator leads to the J dependence of IS in a term of the pure configuration. The J dependence of IS is described by the parameter z_{nl} with the angular coefficient c_{nl} which is the same as that of the spin-orbit radial integral[40,41] ζ_{nl}. For a pure configuration state, the isotope shift including the CSO contributions is thus given by

$$E_{\mathrm{IS}} = d + \sum_k c_k g_k + \sum_{nl} c_{nl} z_{nl}, \tag{46}$$

where d denotes the first-order isotope shift and only depends on the configuration. The intermediate-coupling wavefunction of the state is necessary to calculate the coefficients c_k and c_{nl}. For a configuration of $nl^N(LS')n's(LS)$, equation (46) is written as

$$E_{\mathrm{IS}} = d + cg_l(n's, nl) + c_{nl} z_{nl}, \tag{47}$$

where the coefficients c for the pure LS coupling states have the following simple expressions,[42]

$$c(L, S = S' + \frac{1}{2}) \;=\; -\frac{S'}{2l+1}, \tag{48}$$

$$c(L, S = S' - \frac{1}{2}) \;=\; \frac{S' + 1}{2l + 1}, \tag{49}$$

where S' is the total spin coupled by all electrons of the nl^N shell.

4. Experimental Results

The energy level scheme[31] and the 9 transitions studied are shown in Fig. 7. The ground state of Yb I is $^1S_0$ and has the closed $4f$ shell. Thus, the $(7/2, 3/2)_J$ (J=2,5) and $(7/2,5/2)_5$ states of the $4f^{13}5d6s^2$ configuration are metastable states. The 555.65 nm transition is from the ground state to the $4f^{14}6s6p\ ^3P_1$ state and is a very pure $s^2 - sp$ transition. Another 8 transitions are all from metastable states, where 4 transitions are also $s^2 - sp$ transitions and the other 4 transitions relate to the ^3D_J triplet and $^1D_2$ singlet states of the $4f^{14}6s6d$ configuration. The details about the relevant level energy and the transition energy are given in Table 1.

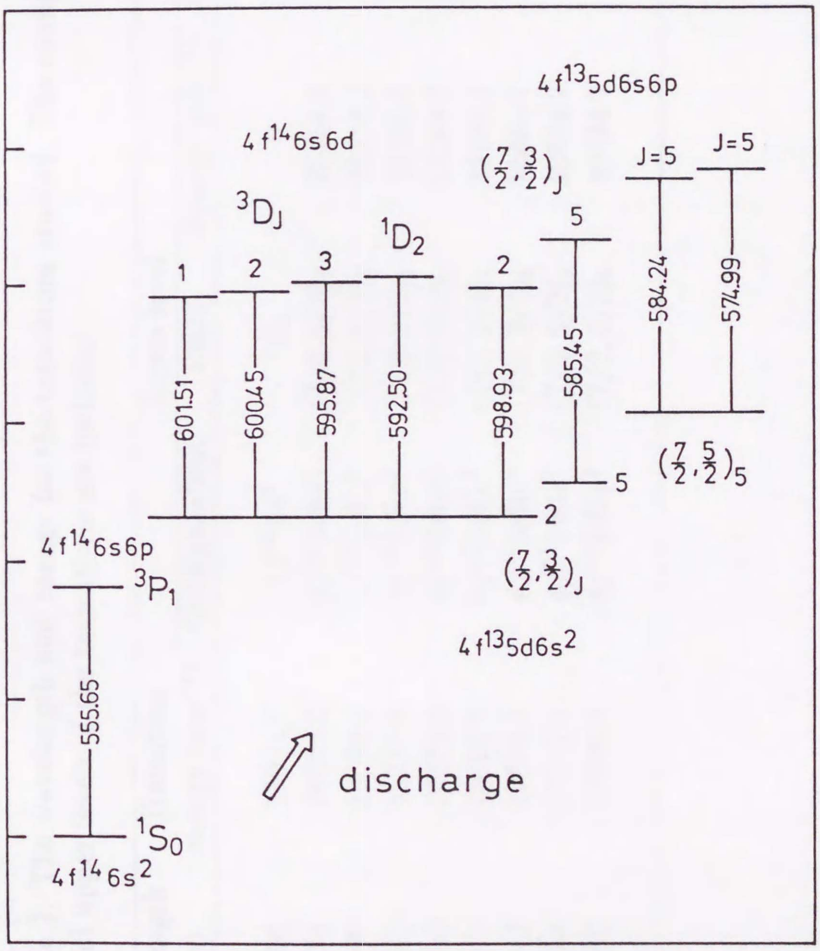

Fig. 7. A level scheme and studied transitions (wavelength in nm) in Yb I. Configuration, term and electronic angular momentum J of levels are given.

Table 1. The wavelength and energy for the transitions studied. The configuration, state and energy of the lower and upper levels of the transitions are included.

Wavelength	Transition	Lower level			Upper level		
(nm)	energy (cm^{-1})	Configuration	State	Energy (cm^{-1})	Configuration	State	Energy (cm^{-1})
555.65	17992.0	$4f^{14}6s^2$	$^1S_0$	0	$4f^{14}6s6p$	$^3P_1$	17992.0
601.51	16620.2	$4f^{13}5d6s^2$	$(7/2,3/2)_2$	23188.5	$4f^{14}6s6d$	$^3D_1$	39808.7
600.45	16649.5	$4f^{13}5d6s^2$	$(7/2,3/2)_2$	23188.5	$4f^{14}6s6d$	$^3D_2$	39838.0
595.87	16777.6	$4f^{13}5d6s^2$	$(7/2,3/2)_2$	23188.5	$4f^{14}6s6d$	$^3D_3$	39966.1
592.50	16873.0	$4f^{13}5d6s^2$	$(7/2,3/2)_2$	23188.5	$4f^{14}6s6d$	$^1D_2$	40061.5
598.93	16691.7	$4f^{13}5d6s^2$	$(7/2,3/2)_2$	23188.5	$4f^{13}5d6s6p$	$(7/2,3/2)_2$	39880.3
585.45	17076.1	$4f^{13}5d6s^2$	$(7/2,3/2)_5$	25859.7	$4f^{13}5d6s6p$	$(7/2,3/2)_5$	42935.8
584.24	17111.4	$4f^{13}5d6s^2$	$(7/2,5/2)_5$	30524.7	$4f^{13}5d6s6p$	J=5	47636.1
574.99	17386.8	$4f^{13}5d6s^2$	$(7/2,5/2)_5$	30524.7	$4f^{13}5d6s6p$	J=5	47911.5

A measured fluorescence spectrum of the 555.65 nm transition from the ground state ${}^1S_0$ of $4f^{14}6s^2$ to the ${}^3P_1$ state of $4f^{14}6s6p$ is shown in Fig. 8. The middle part of Fig. 8 is the fluorescence spectrum and lower part is the simultaneously measured transmitted spectrum of FPI. The spectrum of FPI is very simple and the frequency interval between any two peaks is just equal to the FSR of 297.7 ± 0.2 MHz. Little background is observed for the fluorescence spectrum because the temperature of the Yb oven is very low and the residual radiation background from the oven is effectively

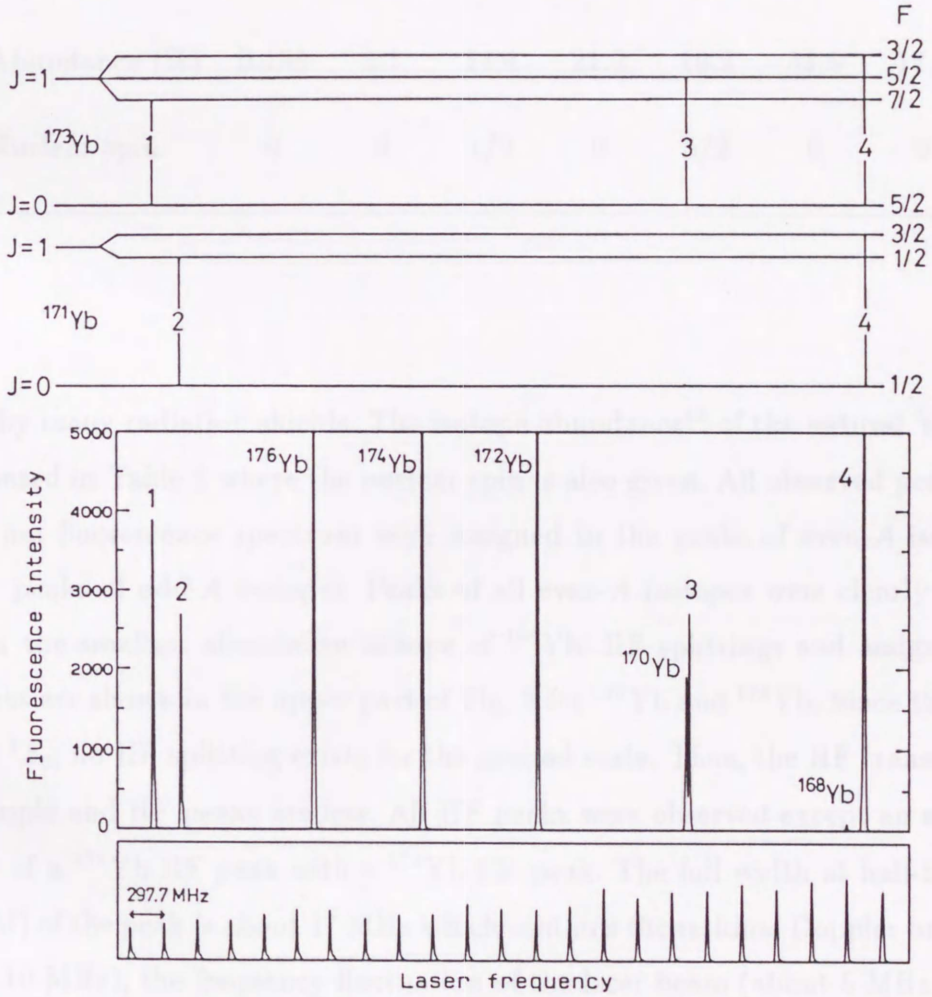

Fig. 8. A fluorescence spectrum (middle part) for the $4f^{14}6s^2\,{}^1S_0 - 4f^{14}6s6p\,{}^3P_1$ transition of 555.65 nm. Peaks of even-A isotopes are labelled with the atomic symbol and HF peaks are numbered. Assignments of HF peaks for ^{171}Yb and ^{173}Yb are shown in the upper part of the figure, where numbers of HF transitions correspond to those on HF peaks. The lower part of the figure is the simultaneously measured transmitted spectrum of FPI.

Table 2. The natural isotopic abundance and the nuclear spin of Yb stable isotopes.

Isotope	^{168}Yb	^{170}Yb	^{171}Yb	^{172}Yb	^{173}Yb	^{174}Yb	^{176}Yb
Abundance (%)	0.135	3.1	14.4	21.9	16.2	31.6	12.6
Nuclear spin	0	0	1/2	0	5/2	0	0

cutted by many radiation shields. The isotope abundance[43] of the natural Yb sample is presented in Table 2 where the nuclear spin is also given. All observed peaks of the 555.65 nm fluorescence spectrum were assigned to the peaks of even-A isotopes or the HF peaks of odd-A isotopes. Peaks of all even-A isotopes were clearly observed even for the smallest abundance isotope of ^{168}Yb. HF splittings and assignments of HF peaks are shown in the upper part of Fig. 8 for ^{171}Yb and ^{173}Yb. Since the ground state is $^1S_0$, no HF splitting exists for the ground state. Thus, the HF transitions are very simple and HF peaks are less. All HF peaks were observed except an accidental overlap of a ^{171}Yb HF peak with a ^{173}Yb HF peak. The full width at half-maximum (FWHM) of the peak is about 17 MHz which contains the residual Doppler broadening (about 10 MHz), the frequency fluctuation of the laser beam (about 5 MHz) and the natural width of the upper level. Thus, the natural width of the upper $^3P_1$ level was estimated to be about 13 MHz.

A measured spectrum of the 592.50 nm transition from the metastable state $(7/2,3/2)_2$ of $4f^{13}5d6s^2$ to the $^1D_2$ state of $4f^{14}6s6d$ is shown in Fig. 9 . A constant background was produced by the electric discharge. Peaks of all even-A isotopes were clearly observed. The odd-A isotope ^{171}Yb with the nuclear spin I=1/2 has a simpler

HF splittings than those of ^{173}Yb with I=5/2. The HF splittings and assignments of the HF peaks for ^{171}Yb and ^{173}Yb are shown in the upper part of Fig. 9. The FWHM of the peak is about 16 MHz and this corresponds to the natural width of the upper level of about 11 MHz.

Peak centers for the fluorescence and FPI spectra were determined by a least squares fitting using a Lorentzian,

$$F(x) = \frac{m_1}{m_2 + (x - m_3)^2}, \tag{50}$$

where m_1, m_2 and m_3 are the parameters to be determined. Fittings by eq. (50) were concentrated on obtaining enough accuracy of the parameter m_3 of the peak center.

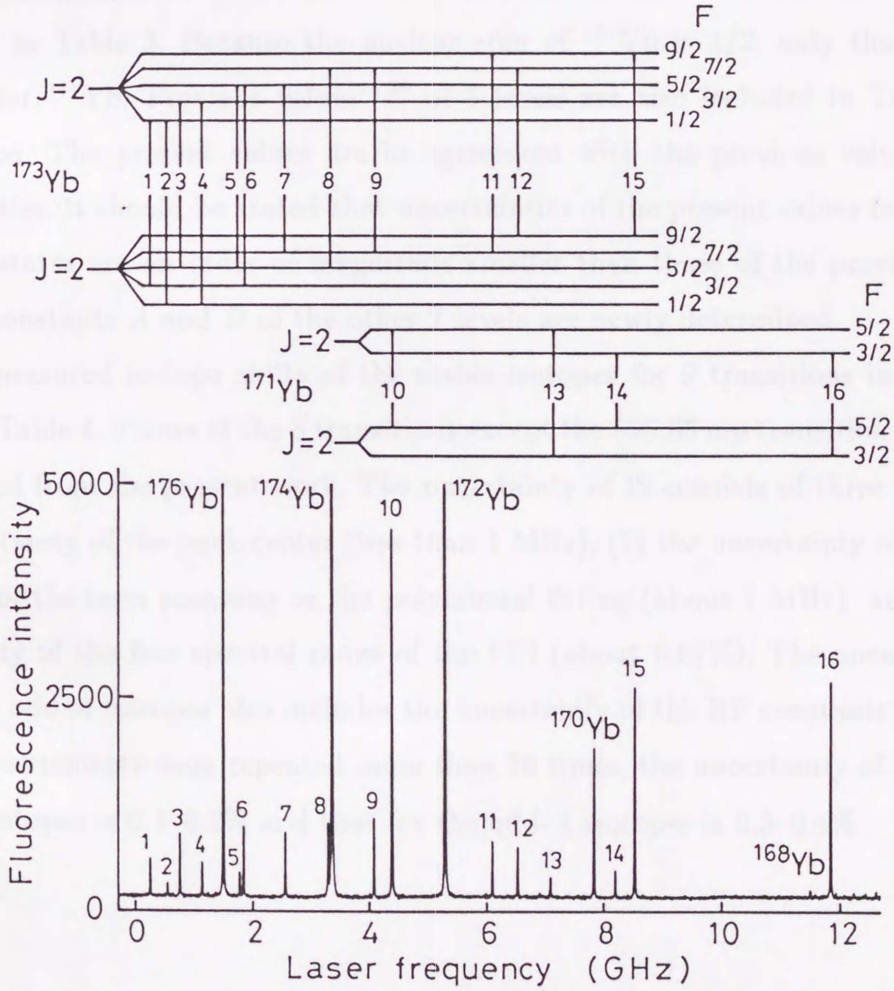

Fig. 9. A fluorescence spectrum for the $4f^{13}5d6s^2$ $(7/2,3/2)_2$ – $4f^{14}6s6d$ $^1D_2$ transition of 592.50 nm. The upper part of the figure is HF splittings and assignments of HF peaks for ^{171}Yb and ^{173}Yb.

Since the frequency interval between any two peaks of FPI spectrum is exactly known, the relation between frequency and channel was obtained from the FPI spectrum by using a least squares fitting with a polynomial. Thus relative frequencies between different peaks were obtained for the fluorescence spectrum. From the HF peaks, the HF splitting energies were obtained, thus the HF coupling constants A and B of the odd-A isotopes were determined both for lower and upper levels of the transition. The center of gravity for odd-A isotopes was also derived from the HF peaks and the determined HF constants A and B. The isotope shifts for the even-A isotopes were obtained from the relative frequencies of the peaks and those of the odd-A isotopes were deduced from the center of gravity.

The determined HF constants A and B of 12 levels for ^{171}Yb and ^{173}Yb are presented in Table 3. Because the nuclear spin of ^{171}Yb is 1/2, only the constant A exists for ^{171}Yb. Previous values[13,26] of 5 levels are also included in Table 3 for comparison. The present values are in agreement with the previous values within uncertainties. It should be stated that uncertainties of the present values for the ^3D_J and $^1D_2$ states are an order of magnitude smaller than those of the previous ones. The HF constants A and B of the other 7 levels are newly determined.

The measured isotope shifts of the stable isotopes for 9 transitions in Yb I are shown in Table 4. Values of the 8 transitions except the 555.65 nm transition are newly determined from the present work. The uncertainty of IS consists of three parts: (1) the uncertainty of the peak center (less than 1 MHz), (2) the uncertainty of the non-linearity of the laser scanning or the polynomial fitting (about 1 MHz), and (3) the uncertainty of the free spectral range of the FPI (about 0.07%). The uncertainty of IS for the odd-A isotopes also includes the uncertainty of the HF constants A and B. Since measurements were repeated more than 10 times, the uncertainty of IS for the even-A isotopes is 0.1–0.2% and that for the odd-A isotopes is 0.3–0.4%.

Table 3. Determined hyperfine constants A and B (MHz) from the present work. Previous values are also included, where values for $^3P_1$ state are from ref. 13 and those for the other states are from ref. 26.

Level	State or J	$A(171)$		$A(173)$		$B(173)$	
(cm^{-1})		Present	Previous	Present	Previous	Present	Previous
17992.0	$^3P_1$	3957.4(29)	3957.97(47)	−1093.97(71)	−1094.20(60)	−826.5(13)	−827.15(47)
23188.5	$(7/2,3/2)_2$	1124.64(40)		−309.64(11)		−1702.50(64)	
25859.7	$(7/2,3/2)_5$	732.91(59)		−201.83(10)		−3036.7(16)	
30524.7	$(7/2,5/2)_5$	648.35(39)		−178.54(7)		−2948.6(13)	
39808.7	$^3D_1$	−2988.5(25)	−2988(25)	818.65(40)	816(20)	59.3(20)	95(40)
39838.0	$^3D_2$	2628.4(15)	2635(15)	−732.49(38)	−725(15)	52.5(23)	80(40)
39880.3	$(7/2,3/2)_2$	3114.6(16)		−860.23(31)		−786.7(21)	
39966.1	$^3D_3$	2026.1(16)	2030(50)	−559.91(47)	−559(30)	139.6(25)	
40061.5	$^1D_2$	−1587.05(92)	−1587(20)	438.45(37)	440(10)	142.2(23)	110(50)
42935.8	$(7/2,3/2)_5$	48.47(14)		−13.32(6)		−1944.6(12)	
47636.1	5	245.46(27)		−66.92(7)		−3813.0(18)	
47911.5	5	1316.47(99)		−363.36(23)		−3049.2(36)	

Table 4. Measured isotope shifts of the stable isotopes for 9 transitions in Yb I.

Transition	Isotope shifts (MHz)					
(nm)	176–174	174–172	172–170	170–168	173–172	171–170
555.65	−953.0(13)	−1001.0(13)	−1285.6(14)	−1369.9(14)	−444.9(14)	−458.8(14)
585.45	−1057.6(12)	−1112.6(12)	−1425.1(14)	−1523.6(16)	−493.7(9)	−508.7(16)
598.93	−1041.2(13)	−1090.0(13)	−1396.3(16)	−1489.6(17)	−485.2(11)	−499.4(19)
584.24	−1228.1(13)	−1285.7(12)	−1647.2(16)	−1756.8(21)	−574.2(8)	−591.5(17)
574.99	−1232.7(14)	−1296.5(15)	−1662.4(18)	−1769.2(18)	−577.7(13)	−596.4(27)
592.50	−1865.4(17)	−1969.9(18)	−2653.6(23)	−2843.3(25)	−848.2(16)	−876.5(17)
595.87	−1835.7(21)	−1938.5(23)	−2606.8(28)	−2802.5(27)	−837.9(30)	−864.9(30)
600.45	−1826.3(21)	−1928.7(22)	−2595.0(26)	−2784.6(27)	−812.7(18)	−847.1(22)
601.51	−1839.9(19)	−1941.9(19)	−2612.2(24)	−2806.6(27)	−858.2(15)	−888.4(21)

5. Analysis and Discussion

5.1 Nuclear parameter λ

To analyse the isotope shift, the modified isotope shift and King plot[1] are usually used. The modified IS $\delta\nu_i^{\mathrm{mod}}$ is defined as

$$\delta\nu_i^{\mathrm{mod}} = (\delta\nu_i - \delta\nu_{i\mathrm{NMS}})\frac{AA'}{A'-A}\cdot\frac{2}{176\cdot 174}, \tag{51}$$

where the NMS is subtracted in the equation. The relation between $\delta\nu_i^{\mathrm{mod}}$ and $\delta\nu_j^{\mathrm{mod}}$ is expressed as

$$\delta\nu_i^{\mathrm{mod}} = \frac{E_i}{E_j}\delta\nu_j^{\mathrm{mod}} + (M_{i\mathrm{SMS}} - \frac{E_i}{E_j}M_{j\mathrm{SMS}})\frac{2}{176\cdot 174}. \tag{52}$$

The plot of $\delta\nu_i^{\mathrm{mod}}$ versus $\delta\nu_j^{\mathrm{mod}}$ is called a King plot which shows a linear relation in absence of the second-order HF perturbation.

The 555.65 nm transition was used as a reference for the King plot, since it is known to be a pure $s^2 - sp$ transition. King plots of the 585.45 nm, 584.24 nm and 592.50 nm transitions are shown in Fig. 10. The 598.93 nm, 574.99 nm and 595.87 nm transitions were not included in Fig.10 because the King plots of these 3 transitions have the same tendencies as the 3 transitions shown in Fig. 10. Very good linear relations were found for these 6 transitions. However, for the 600.45 nm and 601.51 nm transitions, the isotope shifts for the odd-A isotopes were found to deviate largely from the linear relation. Deviations of $\delta\nu_i^{\mathrm{mod}}$ from the linear relation for these 2 transitions are shown in Fig.11. Figure 11 shows that deviations for the even-A isotopes are zero within experimental uncertainties and deviations for the odd-A isotopes are about 40 MHz for the 601.51 nm transition and about −30 MHz for the 600.45 nm transition, respectively. Such deviations may be attributed to the second-order HF perturbation.[44] We tried to explain the deviations considering second-order HF perturbations between the $^3D_1$ and $^3D_2$ states. As a result, the deviations were found to derive mainly from the two states but could not be explained completely. This means that the possibility of the perturbations from other states cannot be excluded. Further measurements are needed to make detailed analysis of second-order HF perturbations.

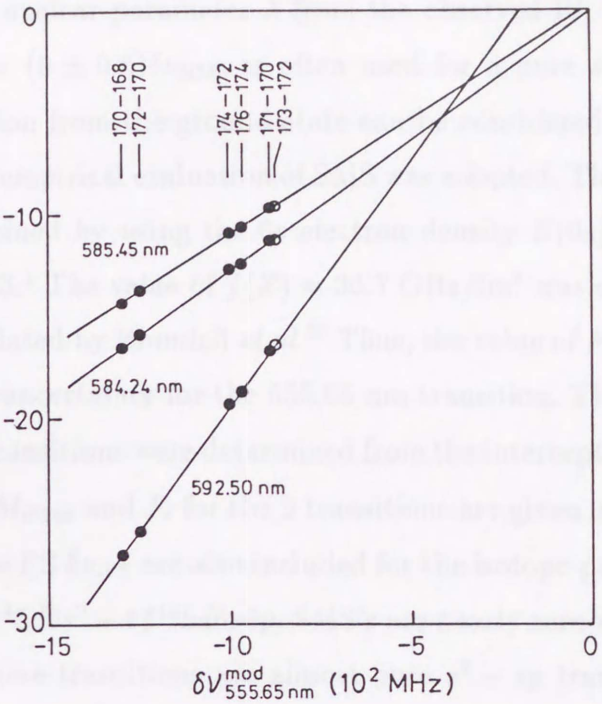

Fig. 10. A King plot of the isotope shifts for the 3 transitions in Yb I. The 555.65 nm transition is taken as a reference. Lines are results by the least squares fitting and experimental uncertainties are within closed circles.

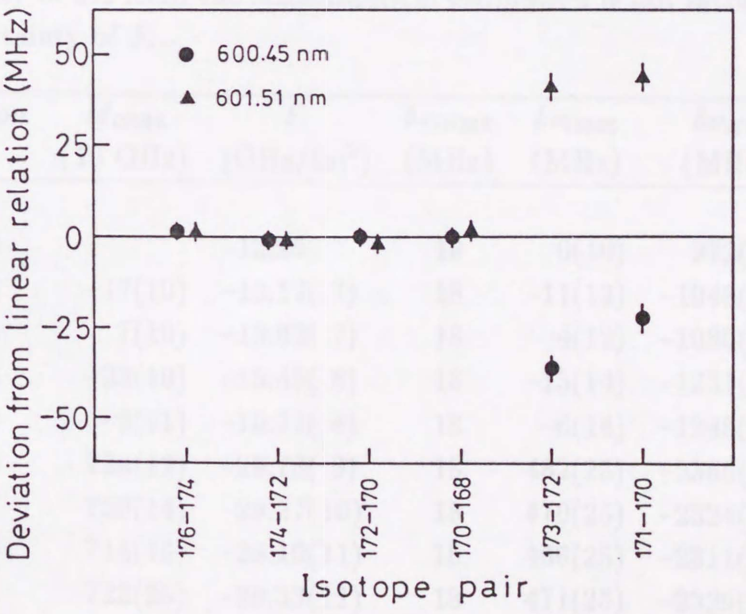

Fig. 11. Deviations of the experimental modified IS from the linear relation in the King plot for the 600.45 nm and 601.51 nm transitions.

To deduce FS and nuclear parameter λ from the observed IS, the semiempirical evaluation[1] of $\delta\nu_{SMS} = (0 \pm 0.5)\delta\nu_{NMS}$ is often used for a pure $s^2 - sp$ transition. The 555.65 nm transition from the ground state can be considered as a pure $s^2 - sp$ transition and the semiempirical evaluation of SMS was adopted. The electronic factor $E_i = E(ns)\gamma$ was obtained by using the 6s electron density $E(6s) = 0.457$ and the screening ratio $\gamma = 0.73$.[1] The value of $f(Z) = 36.7$ GHz/fm^2 was extracted by using the IS constant recalculated by Blundell *et al.*[33] Thus, the value of $F_i = 12.2$ GHz/fm^2 was obtained with 5% uncertainty for the 555.65 nm transition. The values of $M_{i\mathrm{SMS}}$ and F_i for the other 8 transitions were determined from the intercepts and slopes of the King plots. Results of $M_{i\mathrm{SMS}}$ and F_i for the 9 transitions are given in Table 5 in which the SMS $\delta\nu_{i\mathrm{SMS}}$ and the FS $\delta\nu_{i\mathrm{FS}}$ are also included for the isotope pair of 176–174. For the 4 transitions of $4f^{13}5d6s^2 - 4f^{13}5d6s6p$, SMS's are nearly zero within uncertainty and this shows that these transitions are almost pure $s^2 - sp$ transitions. Values of F_i are slightly larger than that of the 555.65 nm transition and this is because the

Table 5. The SMS factor $M_{i\mathrm{SMS}}$ and the electronic factor F_i for the 9 transitions studied . The NMS $\delta\nu_{i\mathrm{NMS}}$, the SMS $\delta\nu_{i\mathrm{SMS}}$ and the FS $\delta\nu_{i\mathrm{FS}}$ are also given for the isotope pair of 176–174. The systematic uncertainty of 5% from the semiempirical estimation is not included in the uncertainty of F_i.

Transition (nm)	$M_{i\mathrm{SMS}}$ (10 GHz)	F_i (GHz/fm^2)	$\delta\nu_{i\mathrm{NMS}}$ (MHz)	$\delta\nu_{i\mathrm{SMS}}$ (MHz)	$\delta\nu_{i\mathrm{FS}}$ (MHz)
555.65		-12.25	19	0(10)	-972(10)
598.93	-17(10)	-13.17(7)	18	-11(12)	-1048(12)
585.45	7(10)	-13.62(7)	18	4(12)	-1080(12)
584.24	-23(10)	-15.49(8)	18	-15(14)	-1231(14)
574.99	-9(11)	-15.71(8)	18	-6(14)	-1245(14)
592.50	736(12)	-29.78(9)	18	482(25)	-2365(25)
595.87	720(14)	-29.27(10)	18	470(25)	-2324(25)
600.45	714(16)	-29.10(11)	18	466(25)	-2311(25)
601.51	722(25)	-29.33(11)	18	471(25)	-2329(25)

screening effect by electrons of $4f^{13}5d$ shells is weaker for the $6s$ electron than that by the electrons of $4f^{14}$ shell. For the 4 transitions of $4f^{13}5d6s^2 - 4f^{14}6s6d$, SMS's are about 470 MHz for a pair of 176–174 and values of F_i are about 30 GHz/fm^2. The 600.45 nm and 601.51 nm transitions were not used for the derivation of λ because the isotope shifts of odd-A isotopes for these 2 transitions deviate from linear relations. Averaged values of λ were obtained from the other 7 transitions.

Derived relative and absolute values of λ are shown in Table 6. The relative value is independent of the electronic factor $E_i f(Z)$ and the uncertainty is less than 0.6% which is due to the uncertainty of IS. The uncertainty of the absolute value is about 5% which is mainly due to the uncertainty of F_i. Previous values from optical,[1] electronic X-ray[45] and muonic X-ray[46] isotope shifts are also included. The λ values from optical and muonic X-ray data in Table 6 were converted from $\delta\langle r^2\rangle$ values by multiplying 0.95 which is the correction factor for the higher order contributions. The present values agree with the optical values and are systematically smaller than the electronic

Table 6. Relative and absolute values of λ from the present work. Previous values are included for comparison.

Isotope pair	Relative λ	Absolute λ (fm^2) Present	Optical^a	Electronic X-ray^b	Muonic X-ray^c
176–174	1.0	0.0794(40)	0.083(12)	0.103(12)	0.102(4)
174–172	1.0492(59)	0.0833(42)	0.087(14)	0.141(13)	0.114(3)
172–170	1.3423(69)	0.1066(53)	0.110(15)	0.163(19)	0.138(5)
170–168	1.4305(73)	0.1136(57)	0.122(18)		
173–172	0.4678(28)	0.0371(19)	0.039(10)	0.050(27)	
171–170	0.4821(29)	0.0383(19)	0.039(10)	0.077(32)	
174–173	0.5815(32)	0.0462(23)		0.091(33)	0.066(5)
172–171	0.8601(41)	0.0683(34)		0.086(14)	0.075(5)

^{a}ref. 1.
^{b}ref. 45.
^{c}ref. 46.

and muonic values. In ref. 13, Clark *et al.* combined the optical IS of the 555.65 nm transition with the electronic and muonic X-ray IS's and derived λ using SMS values of 200–300 MHz for the 555.65 nm transition. This seems unreasonable for a quite pure $s^2 - sp$ transition.[31] It should be noted that the values from the electronic X-ray IS have large uncertainties and values from the muonic X-ray IS are model-dependent.

5.2 $\delta\langle r^2\rangle$ and $\delta\langle\beta^2\rangle$

Changes in mean square nuclear charge radii $\delta\langle r^2\rangle$ and nuclear deformation parameters $\delta\langle\beta^2\rangle$ have been derived for $^{168-176}$Yb from values of λ by using the two parameter model and are given in Table 7. Using the optical values of λ and the $B(E2)$ values from Coulomb excitation experiments, we deduced values of $\delta\langle r^2\rangle$, $\delta\langle r^4\rangle$ and $\delta\langle r^6\rangle$. Results of $\delta\langle r^2\rangle$, $\delta\langle r^4\rangle$ and $\delta\langle r^6\rangle$ are also given in Table 7

Table 7. Changes in mean square nuclear charge radii $\delta\langle r^2\rangle$, nuclear deformation parameters $\delta\langle\beta^2\rangle$, and higher order terms $\delta\langle r^4\rangle$ and $\delta\langle r^6\rangle$ for the stable isotopes of Yb.

Isotope pair	Two-parameter model		Numerical analysis		
	$\delta\langle r^2\rangle$ (fm^2)	$\delta\langle\beta^2\rangle$ (10^{-3})	$\delta\langle r^2\rangle$ (fm^2)	$\delta\langle r^4\rangle$ (10 fm^4)	$\delta\langle r^6\rangle$ (10^3 fm^6)
176–174	0.0833(43)	–2.20(39)	0.0848(46)	0.734(40)	0.554(30)
174–172	0.0875(45)	–1.80(41)	0.0888(46)	0.731(38)	0.514(27)
172–170	0.1124(57)	0.52(53)	0.1135(66)	0.915(54)	0.617(36)
170–168	0.1200(61)	1.24(57)	0.1210(72)	0.984(59)	0.687(41)
173–172	0.0389(20)	–1.35(18)			
171–170	0.0401(21)	–1.23(19)			

in which only values for even-A isotopes are presented because the reliable $B(E2)$ values[47] are available only for the even-A isotopes. From Table 7, it can be seen that the $\delta<r^2>$ values from the two-parameter model are in agreement with those from the numerical analysis. This means that the two-parameter model is a good approximation to extract $\delta<r^2>$.

Combining the present results for Yb stable isotopes with our previous results[14,15] for Nd, Sm, Gd, Dy and Er stable isotopes, we obtained the systematic trends of $\delta<r^2>$ and $\delta<\beta^2>$ for the neutron number of N=82–106. Figure 12 shows the sys-

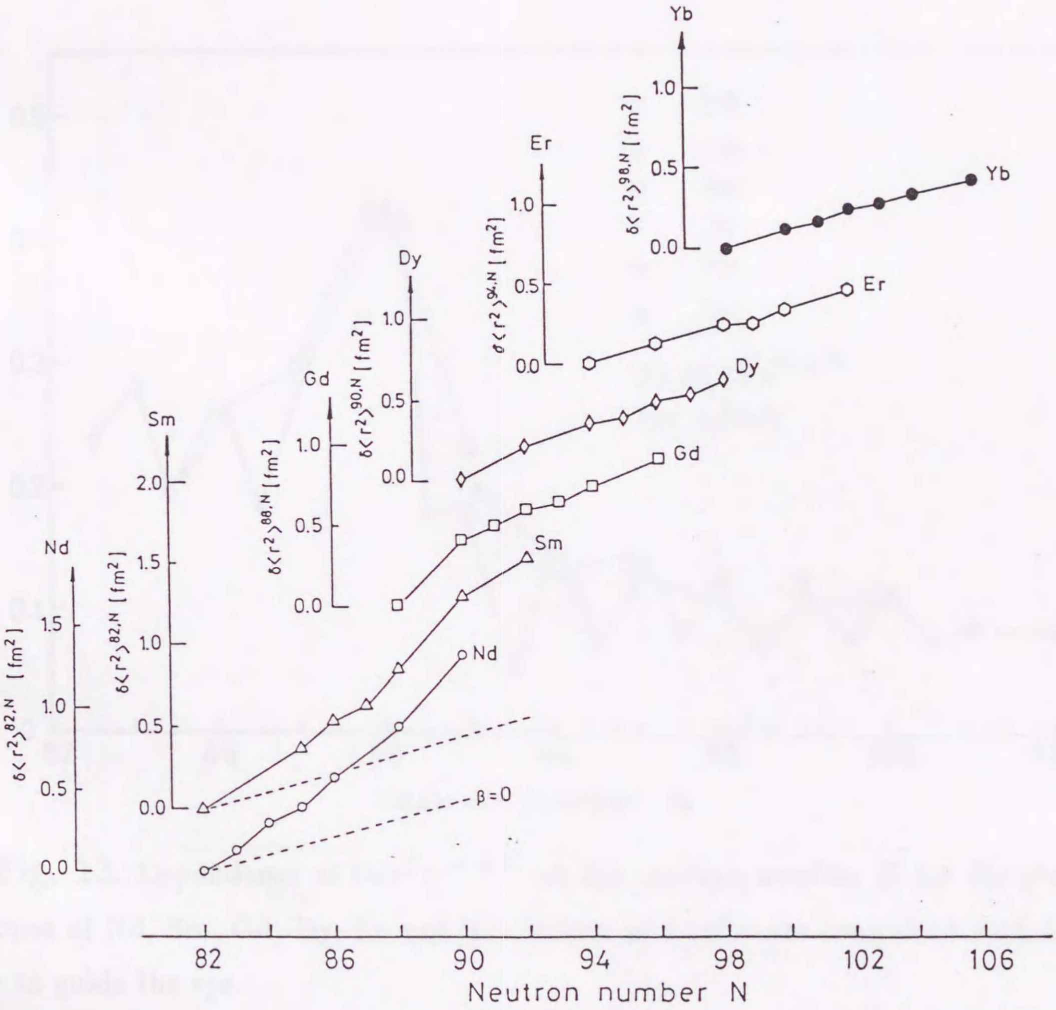

Fig. 12. Systematics of $\delta<r^2>$ for the stable isotopes of Nd, Sm, Gd, Dy, Er and Yb. Normalizations were carrried out at the isotope with the smallest neutron number N for each element. Dashed line is the change of $\delta<r^2>$ for a spherical nucleus calculated by the droplet model.

tematic change of $\delta<r^2>$ for the neutron number of 82–106, where values of $\delta<r^2>$ are normalized to 0 at the isotope with the smallest neutron number for each element. The dashed line is the value of $\delta<r^2>$ for a spherical nucleus calculated by using the droplet model.[34] From Fig. 12, it can be seen that the values of $\delta<r^2>$ change rapidly at N=88–90 and the change of $\delta<r^2>$ becomes almost parallel to the dashed line above N=94. This drastical change of $\delta<r^2>$ at N=88–90 is clearly seen in Fig. 13 which shows the systematic change of $\delta<r^2>^{N-2,N}$. It is also seen from Fig. 13 that the values of $\delta<r^2>^{N-2,N}$ reduce very smoothly above N=94. The systematic

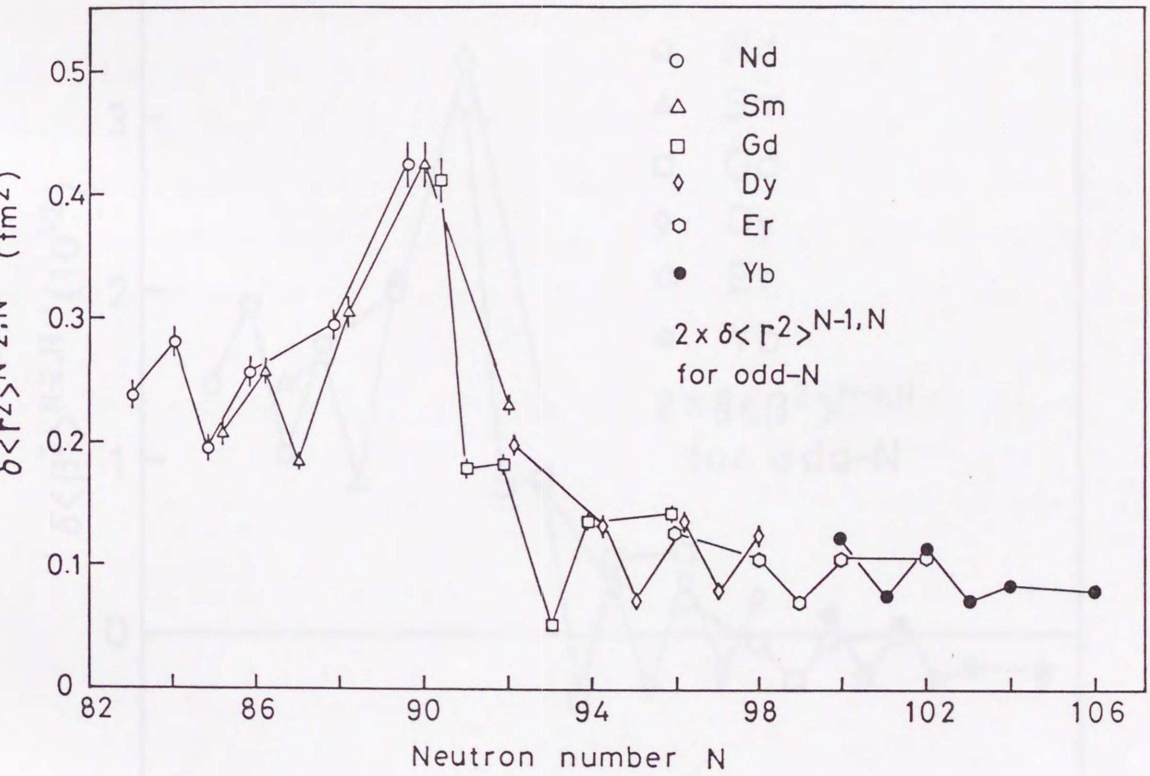

Fig. 13. Dependence of $\delta<r^2>^{N-2,N}$ on the neutron number N for the stable isotopes of Nd, Sm, Gd, Dy, Er and Yb. Values of $\delta<r^2>$ are connected with lines only to guide the eye.

change of $\delta<\beta^2>^{N-2,N}$ is shown in Fig. 14 for N=82–106. Figure 14 shows that the values of $\delta<\beta^2>$ are very large around N=88–90 and become small above N=94. The values of $\delta<\beta^2>$ are nearly zero around N=100–102 and are negative at N=104 and 106. That is, the values of $\delta<\beta^2>$ reduce slowly from positive to negative. This means that the nuclear shape changes from spherical (vibrational) to deformed one around N=88–90 and the nuclei with N=100–102 have very stable quadrupole deformation. It is also shown that deformation reduces a little at N=104 and 106.

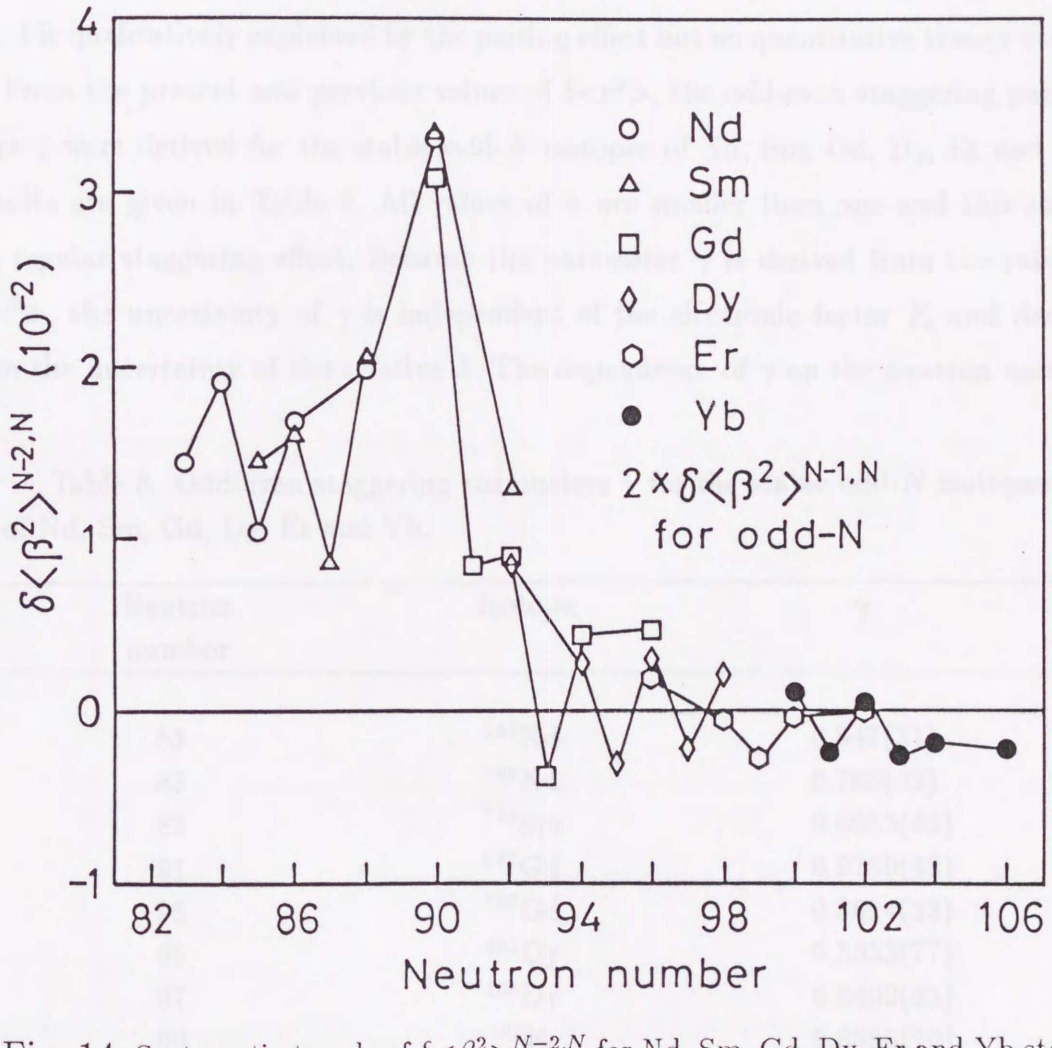

Fig. 14. Systematic trends of $\delta<\beta^2>^{N-2,N}$ for Nd, Sm, Gd, Dy, Er and Yb stable isotopes. Values of $\delta<\beta^2>$ are connected with lines only to guide the eye.

It has been known from the early days of IS measurements that the value of $<r^2>$ for an odd-N nucleus is smaller than the average value of $<r^2>$ for its even-N neighbors for the general case. This effect is called the odd-even staggering effect[6] and is described by the staggering parameter γ as follows:

$$\gamma = \frac{2\delta < r^2 >^{N-1,N}}{\delta < r^2 >^{N-1,N+1}}, \tag{53}$$

where N is odd. The regular odd-even staggering effect is expressed by $\gamma < 1$ (recently the irregular staggering effect of $\gamma > 1$ was also observed[4]). The staggering effect of $\gamma < 1$ is qualitatively explained by the pairing effect but no quantitative theory exists.

From the present and previous values of $\delta<r^2>$, the odd-even staggering parameters γ were derived for the stable odd-N isotopes of Nd, Sm, Gd, Dy, Er and Yb. Results are given in Table 8. All values of γ are smaller than one and this shows the regular staggering effect. Because the parameter γ is derived from the ratio of $\delta<r^2>$, the uncertainty of γ is independent of the electronic factor F_i and derives from the uncertainty of the relative λ. The dependence of γ on the neutron number

Table 8. Odd-even staggering parameters γ for the stable odd-N isotopes of Nd, Sm, Gd, Dy, Er and Yb.

Neutron number	Isotope	γ
83	^{143}Nd	0.847(31)
85	^{145}Nd	0.763(32)
87	^{149}Sm	0.6053(43)
91	^{155}Gd	0.9780(48)
93	^{157}Gd	0.3824(33)
95	^{161}Dy	0.5333(77)
97	^{163}Dy	0.6400(85)
99	^{167}Er	0.6895(70)
101	^{171}Yb	0.7135(58)
103	^{173}Yb	0.8891(76)

N is shown in Fig. 15. It is seen from Fig. 15 that the value of γ reduces with the neutron number N for N=83–87 and increases for N=93–103. A large value of $\gamma \sim 1$ is found at N=91. This means that the staggering effect becomes stronger, with N, near the spherical region (N=82) and becomes weaker for the well deformed nucleus (above N=94). The large value of γ at N=91 shows that the nuclear shape change at about N=90 is dominant and the staggering effect is small.

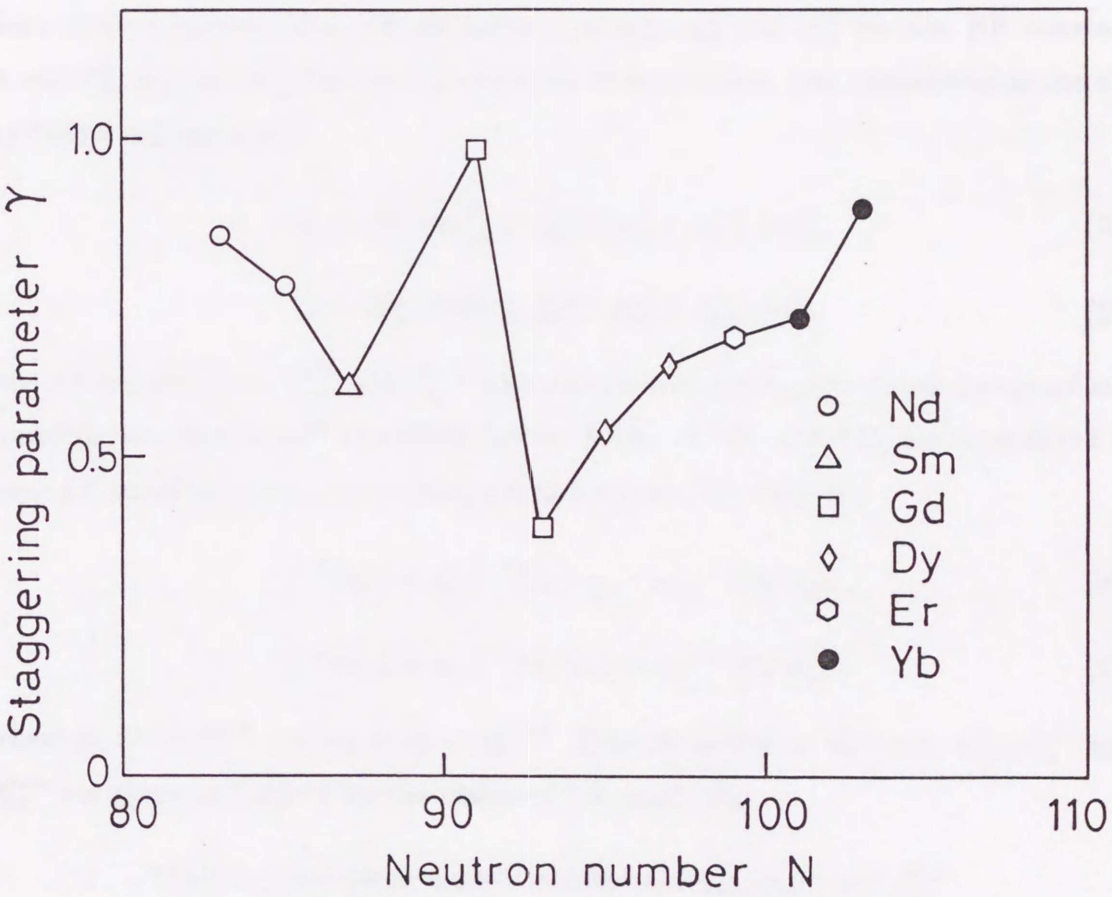

Fig. 15. Dependence of the odd-even staggering parameter γ on the neutron number N for the stable odd-N isotopes of Nd, Sm, Gd, Dy, Er and Yb.

5.3 Single-electron HF parameters for the $4f^{14}6s6d$ configuration

To obtain the single-electron HF parameters of $6s$ and $6d$ electrons, we carried out the parametric analysis of the effective operator procedure for the HF constants A and B of the ^3D_J and $^1D_2$ states of the $4f^{14}6s6d$ configuration. Parameters of the $4f$ electron need not to be considered for the Yb I $4f^{14}6s6d$ configuration, because electrons of the closed $4f$ shell couple to the $^1S_0$ term.[31] The parameter a_{6d}^{10} for the HF constant A was omitted because a_{6d}^{10} is known to be very small ($\sim a_{6d}^{01}/50$).[16] Thus, both three single-electron HF parameters of a_{6d}^{01}, a_{6d}^{12} and a_{6s}^{10} for the HF constant A and b_{6d}^{02}, b_{6d}^{13} and b_{6d}^{11} for the HF constant B were taken into consideration for the $4f^{14}6s6d$ configuration.

$$A = \alpha_{6d}^{01}(J)a_{6d}^{01} + \alpha_{6d}^{12}(J)a_{6d}^{12} + \alpha_{6s}^{10}(J)a_{6s}^{10}, \tag{54}$$

$$B = \beta_{6d}^{02}(J)b_{6d}^{02} + \beta_{6d}^{13}(J)b_{6d}^{13} + \beta_{6d}^{11}(J)b_{6d}^{11}, \tag{55}$$

where the coefficients $\alpha_{nl}^{k_s k_l}$ and $\beta_{nl}^{k_s k_l}$ were calculated by using the simple intermediate-coupling wavefunctions[26] described below. States of $^3D_1$ and $^3D_3$ are considered as pure LS coupling states but mixing exists between $^3D_2$ and $^1D_2$.

$$|\ ^3D_2 >= \alpha_1 \ |\ ^3D_2 >_{LS} - \alpha_2 \ |\ ^1D_2 >_{LS}, \tag{56}$$

$$|\ ^1D_2 >= \alpha_1 \ |\ ^1D_2 >_{LS} + \alpha_2 \ |\ ^3D_2 >_{LS}, \tag{57}$$

where $\alpha_1 = 0.926$[26] and $\alpha_2 = (1-\alpha_1^2)^{1/2}$. The calculated coefficients α_{6s}^{10}, $\alpha_{6d}^{k_s k_l}$ and $\beta_{6d}^{k_s k_l}$ are given in Table 9 for the states of ^3D_J and $^1D_2$.

Table 9. Calculated angular coefficients α_{6s}^{10}, $\alpha_{6d}^{k_s k_l}$ and $\beta_{6d}^{k_s k_l}$ for the ^3D_J and $^1D_2$ states of the $4f^{14}6s6d$ configuration.

State	α_{6s}^{10}	α_{6d}^{01}	α_{6d}^{12}	β_{6d}^{02}	β_{6d}^{13}	β_{6d}^{11}
$^3D_1$	-0.2500	1.5000	0.5000	0.2000	0.0490	-0.0200
$^3D_2$	0.2143	0.8571	0.2857	0.3256	0.1000	-0.0000
$^3D_3$	0.1667	0.6667	-0.0952	0.5714	-0.0350	0.1333
$^1D_2$	-0.1310	0.9762	-0.1191	0.5306	-0.0300	0.0667

The HF constants A of ^{171}Yb and constants A and B of ^{173}Yb for the ^3D_J and $^1D_2$ states of $4f^{14}6s6d$ were fitted by eqs. (54) and (55). The obtained single-electron HF parameters are given in Table 10. The value of a_{6s}^{10} for the ^{173}Yb I $4f^{14}6s6p$ configuration obtained by Clark *et al.*[13] is also included in Table 10, and the absolute value is somewhat smaller than the present result for the $4f^{14}6s6d$ configuration. The reason is that the screening effect by the $6p$ electron in the $4f^{14}6s6p$ configuration is stronger for the $6s$ electron than that by the $6d$ electron in the $4f^{14}6s6d$ configuration. It can also be seen from Table 10 that the contribution of the $6s$ electron is dominant for the HF constant A.

Deviations of fitted values by eqs. (54) and (55) from experimental values of A and B are shown in Fig. 16. Only deviations for ^{173}Yb are shown in the figure since deviations for ^{171}Yb have the same tendency as those for ^{173}Yb. Figure 16 shows that deviations of A and B are nearly within uncertainties. This means the fit is reasonable. Although the second-order HF perturbation was found for the $^3D_1$ and $^3D_2$ states of $4f^{14}6s6d$ from the deviation of the isotope shifts from the King plot, influence of such perturbation on HF constants A and B could not be observed at the present uncertainty.

Table 10. Single-electron hyperfine parameters (MHz) of the $4f^{14}6s6d$ configuration in Yb I. Reference value of a_{6s}^{10} is also given for the ^{173}Yb I $4f^{14}6s6p$ configuration.

Isotope	a_{6d}^{01}	a_{6d}^{12}	a_{6s}^{10}	b_{6d}^{02}	b_{6d}^{13}	b_{6d}^{11}
^{171}Yb	10.88(76)	60.6(34)	12143(5)			
^{173}Yb	-4.81(26)	-28.49(88)	-3360(1)	311.6(76)	-432(35)	-446(49)
			-2815[a]			

[a]ref. 13.

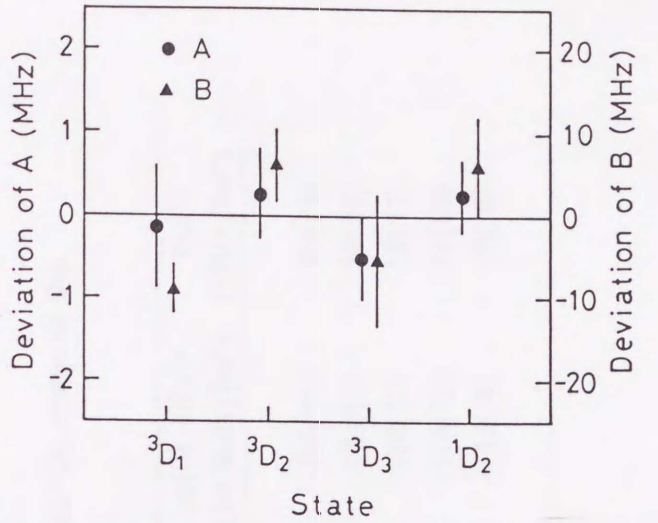

Fig. 16. Deviations of fitted values of HF constants A and B for ^{173}Yb from experimental values for the ^3D_J and $^1D_2$ states of the $4f^{14}6s6d$ configuration.

5.4 J and term dependences of IS and CSO effects for the ^3D_J and $^1D_2$ states of $4f^{14}6s6d$

For the ^3D_J and $^1D_2$ states of $4f^{14}6s6d$, we introduce the residual isotope shift $T_{\rm res}$ of a state which is a difference in the level IS relative to that of the $^3D_1$ state. The NMS is subtracted in $T_{\rm res}$. Values of $T_{\rm res}$ were obtained for the ^3D_J and $^1D_2$ states from the 4 transitions of $4f^{13}5d6s^2$–$4f^{14}6s6d$ which share the same lower state $(7/2,3/2)_2$. Results are shown in Table 11 where only values for even-A isotopes are given, because the isotope shifts for odd-A isotopes deviate from linear relations as shown in §5.1. J and term dependences can be found for the ^3D_J and $^1D_2$ states from values of $T_{\rm res}$ in Table 11.

As discussed in §5.3, there is a mixing between $^3D_2$ and $^1D_2$ states. Thus, the measured values of $T_{\rm res}$ are written as

$$T_{\rm res}(^3D_3) = \delta E_{\rm IS} = \delta c_{6d} z_{6d}, \tag{58}$$

$$T_{\rm res}(^3D_2 \text{ or } ^1D_2) = \delta c g_2(6s, 6d) + \delta c_{6d} z_{6d}, \tag{59}$$

where the coefficients c and c_{6d} were calculated by using the intermediate-coupling wavefunction[26] and are presented in Table 12 for the ^3D_J and $^1D_2$ states of $4f^{14}6s6d$.

Table 11. Residual isotope shifts and CSO parameters for the ^3D_J and $^1D_2$ states of the $4f^{14}6s6d$ configuration.

Isotope	Residual isotope shift (MHz)				$g_2(6s,6d)$	z_{6d}	$g_2(6s,6d)/\lambda$	z_{6d}/λ
pair	$^3D_1$	$^3D_2$	$^3D_3$	$^1D_2$	(MHz)	(MHz)	(10 MHz/fm^2)	(MHz/fm^2)
176–174	0	13.5(29)	4.0(28)	−25.8(26)	−86(11)	1.6(11)	−108(15)	20(14)
176–172	0	26.8(46)	7.3(48)	−54.0(44)	−177(18)	2.9(19)	−109(12)	18(12)
176–170	0	43.9(72)	12.5(72)	−95.8(70)	−313(28)	5.0(29)	−116(12)	19(11)
176–168	0	65.9(98)	16.4(99)	−132.8(98)	−431(39)	6.6(40)	−113(12)	17(10)
Average							−112(6)	18(6)

Table 12. Calculated angular coefficients c and c_{6d} for the ^3D_J and $^1D_2$ states of the $4f^{14}6s6d$ configuration.

State	$^3D_1$	$^3D_2$	$^3D_3$	$^1D_2$
c	-0.1000	-0.0428	-0.1000	0.2428
c_{6d}	-1.5000	-1.2858	1.0000	0.7858

The CSO parameters $g_2(6s,6d)$ and z_{6d} were obtained from $T_{\rm res}$ of $^3D_3$ and $^1D_2$ and results are also shown in Table 11. $T_{\rm res}$ of the $^3D_2$ state could not be reproduced by eq. (59). This suggests that the configuration mixing exists for this level. Mixing with the $(7/2,3/2)_2$ state of the $4f^{13}5d6s6p$ configuration is possible because the energy of the state is 39880 cm^{-1} which is close to the energy of 39838 cm^{-1} of the $4f^{14}6s6d$ $^3D_2$ state. To compare the parameters $g_2(6s,6d)$ and z_{6d} for different isotope pairs, these values are divided by nuclear parameters λ and results are given in Table 11. Values of $g_2(6s,6d)/\lambda$ and z_{6d}/λ are constant within uncertainties as seen in Table 11. This means that the FS has dominant contribution in the CSO effects both for the electrostatic and magnetic interactions. The averaged values of -1120(60) MHz/fm^2 for $g_2(6s,6d)/\lambda$ and 18(6) MHz/fm^2 for z_{6d}/λ were obtained.

For comparing the present value of z_{6d} with the z_{5d} values of other elements, we used the normalized parameter $z_{nl,\rm norm} = z_{nl}/\lambda\zeta_{nl}$. The present value of $z_{6d,\rm norm}$ for the Yb I $4f^{14}6s6d$ configuration was obtained and is given in Table 13 which also includes values of $z_{5d,\rm norm}$ for the Gd I $4f^7 5d6s^2$ configuration (our previous value[16]), $z_{5d,\rm norm}$ for the Gd II $4f^7 5d6s$ configuration and $z_{5d,\rm norm}$ for the Eu I $4f^7 5d6s$ configuration. From Table 13, it is seen that the parameters of $z_{6d,\rm norm}$ and $z_{5d,\rm norm}$ are constant within experimental uncertainties. It seems that values of $z_{nl,\rm norm}$ are constant not only for the $5d$ electrons[16] but also for the $6d$ electrons for the rare-earth elements. For the parameter z_{4f} of some rare-earth elements, values of $z_{4f,\rm norm}$ were shown to increase with the atomic number as the spin-orbit integral[25] ζ_{4f}. However, values of the parameters $z_{5d,\rm norm}$ for different elements seem to scatter for the ground configuration $(5d+6s)^N$ in the series of $5d$ elements.[53]

Table 13. Comparison of the present value of the CSO parameter $z_{6d,\mathrm{norm}}$ with the previous values of $z_{5d,\mathrm{norm}}$.

Configuration	Electron shell nl	z_{nl} (MHz)	λ (fm^2)	z_{nl}/λ ($\mathrm{MHz/fm}^2$)	ζ_{nl} (cm^{-1})	$z_{nl,\mathrm{norm}}$ ($10^{-6}\ \mathrm{fm}^{-2}$)
Yb I $4f^{14}6s6d$	$6d$			18(6)	63[f]	9.5(32)
Gd I $4f^7 5d6s^2$	$5d$			134(4)[e]	710(64)[g]	6.29(60)
Gd II $4f^7 5d6s$	$5d$	42(11)[a]	0.265(10)[c]	158(42)	832(28)[h]	6.3(17)
Eu I $4f^7 5d6s$	$5d$	43.6(59)[b]	0.552(25)[d]	79(11)	389[a]	6.77(97)

[a]ref. 48, [b]ref. 22, [c]ref. 14,
[d]ref. 49, [e]ref. 16, [f]ref. 50,
[g]ref. 51, [h]ref. 52.

6. Conclusion

To get information about nuclear and electronic properties, we measured isotope shifts and hyperfine structures in Yb I by means of atomic-beam laser spectroscopy. The experimental setup of atomic-beam laser spectroscopy was shown to have enough energy resolution and counting efficiency to record IS and HFS spectra. Isotope shifts and hyperfine structures of 9 transitions were measured for the stable isotopes with A=168–176. One transition is directly from the ground state and the other 8 transitions are from metastable states which were measured for the first time. The electric discharge was developed to populate the metastable states in Yb I. Detailed conditions to maintain the stable electric discharge were examined. Dependences of populations for the ground and metastable states on the discharge current and voltage were investigated. Intense population of the metastable states were achieved up to 70% by the electric discharge.

From HFS, HF constants A and B of 12 levels were determined for ^{171}Yb and ^{173}Yb of which 7 levels were newly determined. For the ^3D_J and $^1D_2$ states of the $4f^{14}6s6d$ configuration, HF constants A for ^{171}Yb and A and B for ^{173}Yb were analyzed with the effective operator procedure and single-electron HF parameters a^{10}_{6s}, a^{01}_{6d}, a^{12}_{6d} and b^{02}_{6d}, b^{13}_{6d}, b^{11}_{6d} of $6s$ and $6d$ electrons were derived. The $6s$ electron was found to have dominant contribution to the constant A. The parameters of $6d$ electron were deduced for the first time.

From IS, reliable nuclear parameters λ were obtained and found to be in agreement with the values from the previous optical IS and systematically smaller than the values from electronic and muonic X-ray IS's. Changes in mean square nuclear charge radii $\delta<r^2>$ were deduced using both the two-parameter model and the numerical analysis. The values obtained with these two methods agreed quite well. Higher order terms $\delta<r^4>$ and $\delta<r^6>$ were also determined with the numerical analysis for the even-A isotopes. It was found that Yb isotopes with A=170 and 172 have very stable quadrupole deformation and deformation reduces a little for the isotopes with A=174 and 176. The odd-even staggering effect was discussed for the odd-N isotopes.

For the ^3D_J and $^1D_2$ states of the $4f^{14}6s6d$ configuration, J and term dependences of IS were examined and they were attributed to the CSO effect. CSO parameters of $g_2(6s, 6d)/\lambda$=−1120(60) MHz/fm^2 and z_{6d}/λ = 18(6) MHz/fm^2 were derived for the first time. The value of z_{6d}/λ was compared with the values of $5d$ electrons of other elements and was found to be proportional to the spin-orbit integral ζ_{nl} just as that of $5d$ electrons. The field shift was found to be dominant in the CSO effect both for the electrostatic and magnetic interactions.

For the $^3D_1$ and $^3D_2$ states of the $4f^{14}6s6d$ configuration, isotope shifts related to these two states were found to largely deviate from the King plot. We concluded that this deviation is caused by the second-order HF perturbation. However, influence of this perturbation on HF constants A and B was not observed within present uncertainty. Since other levels should be involved into the second-order HF perturbation, detailed analysis of this deviation for the $^3D_1$ and $^3D_2$ states of $4f^{14}6s6d$ was not done at the present work.

Acknowledgment

I would like to express my sincere appreciations to Professor Yasukazu Yoshizawa for his valuable advice and strong encouragement, and to Professor Ichta Endo for his useful guidance and critical reading of this thesis. I am particularly grateful to Dr. Takayoshi Horiguchi for his continuous support and detailed suggestions. I am also indebted to many students of our group, Dr. Masanori Wakasugi, Mr. Takashi Hasegawa and Ms. Wei Yang. I would like to thank all members of Department of Physics, Faculty of Science for their hospitalities during my study and life in Hiroshima. I greatly appreciate the fellowship from the Ministry of Education, Science and Culture of Japan during my stay at Hiroshima University.

References

1. K. Heilig and A. Steudel: At. Data Nucl. Data Tables **14** (1974) 613.
2. W.J. Childs: Case Stud. At. Phys. **3** (1973) 215.
3. *High-Resolution Laser Spectroscopy*, ed. K. Shimoda (Springer-Verlag, Berlin, 1976).
4. S.A. Ahmad, W. Klempt, R. Neugart, E.W. Otten, P.-G. Reinhard, G. Ulm and K. Wendt: Nucl. Phys. **A483** (1988) 244.
5. A.C. Mueller, F. Buchinger, W. Klempt, E.W. Otten, R. Neugart, C. Ekström and J. Heinemeier: Nucl. Phys. **A403** (1983) 234.
6. E.W. Otten: *Treatise on Heavy-Ion Science*, ed. D.Allan Bromley (Plenum Press, New York, 1989)Vol. 8, p. 517.
7. W.J. Childs and L.S. Goodman: Phys. Rev. **A6** (1972) 1772.
8. W.J. Childs, O. Poulsen and L.S. Goodman: Phys. Rev. **A19** (1979) 160.
9. H. Brand, V. Pfeufer and A. Steudel: Z. Phys. **A302** (1981) 291.
10. W.J. Childs: Phys. Rev. **A39** (1989) 4956.
11. G.J. Zaal, W. Hogervorst, E.R. Eliel, K.A.H.van Leeuwen and J. Blok: J. Phys. **B13** (1980) 2185.
12. A. Bernard, H. Brüggemeyer and V. Pfeufer: Z. Phys. **A322** (1985) 1.
13. D.L. Clark, M.E. Cage, D.A. Lewis and G.W. Greenlees: Phys. Rev. **A20** (1979) 239.
14. M. Wakasugi, T. Horiguchi, W.G. Jin, H. Sakata and Y. Yoshizawa: J. Phys. Soc. Jpn. **59** (1990) 2700.
15. W.G. Jin, T. Horiguchi, M. Wakasugi and Y. Yoshizawa: J. Phys. Soc. Jpn. **59** (1990) 3148.

16. W.G. Jin, H. Sakata, M. Wakasugi, T. Horiguchi and Y. Yoshizawa: Phys. Rev. **A42** (1990) 1416.

17. A.A. Radzig and B.M. Smirnov: *Reference Data on Atoms, Molecules and Ions* ed. J.P. Toennies (Springer-Verlag, Berlin, 1985).

18. W.J. Childs, L.S. Goodman and V. Pfeufer: Phys. Rev. **A28** (1983) 3402.

19. P.G.H. Sandars and J. Beck: Proc. R. Soc. London, Ser. **A289** (1965) 97.

20. V. Pfeufer: Z. Phys. **D4** (1987) 351.

21. J. Bauche and R.-J. Champeau: Adv. At. Mol. Phys. **12** (1976) 39.

22. P. Seifert, D.-J. Weber, H.-D. Kronfeldt and R. Winkler: Z. Phys. **D14** (1989) 99.

23. H. Brüggemeyer, H. Esrom, V. Pfeufer, A. Steudel and J. Bauche: Z. Phys. **D1** (1986) 55.

24. V. Pfeufer, W.J. Childs and L.S. Goodman: J. Phys. **B16** (1983) L557.

25. H.-D. Kronfeldt and G. Sinn: Z. Phys. **D14** (1989) 205.

26. M. Baumann and M. Braun: Z. Phys. **D1** (1986) 247.

27. W.J. Childs and L.S. Goodman: Phys. Rev. **A3** (1971) 25.

28. S. Gerstenkorn and P. Luc: *Atlas du spectre d'absorption de la molecule d'iode* (Editions du CNRS, Orsay, France, 1978).

29. S. Ishii and W. Ohlendorf: Rev. Sci. Instrum. **43** (1972) 1632.

30. W.G. Jin, T. Horiguchi, M. Wakasugi, T. Hasegawa and W. Yang: Jpn. J. Appl. Phys. **30** (1991) 1139.

31. W.C. Martin, R. Zalubas and L. Hagan: *Atomic Energy Levels–The Rare-Earth Elements*, NSRDS-NBS60 (U.S. GPO, Washington, D.C., 1978).

32. E.C. Seltzer: Phys. Rev. **188** (1969) 1916.

33. S.A. Blundell, P.E.G. Baird, C.W.P. Palmer, D.N. Stacey, G.K. Woodgate and D. Zimmermann: Z. Phys. **A321** (1985) 31.

34. W.D. Myers and K.-H. Schmidt: Nucl.Phys. **A410** (1983) 61.

35. E.R. Eliel, W. Hogervorst, G.J. Zaal, K.A.H.van Leeeuwen and J. Blok: J. Phys. **B13** (1980) 2195.

36. I. Lindgren and A. Rosén: Case Stud. At. Phys. **4** (1974) 93.

37. A.R. Edmonds: *Angular Momentum in Quantum Mechanics* (Princeton University Press, Princeton, 1960).

38. H. Kopfermann: *Nuclear Moments* (Academic Press, New York, 1958).

39. W.J. Childs: Phys. Rev. **A2** (1970) 316.

40. J.C. Slater: *Quantum Theory of Atomic Structure* (Mcgraw-hill Book Company, New York, 1960).

41. E.U. Condon and G.H. Shortley: *The Theory of Atomic Spectra* (Cambridge University Press, Cambridge, 1935).

42. P. Aufmuth: J. Phys. **B15** (1982) 3127.

43. Y. Yoshizawa, T. Horiguchi and M. Yamada: *Chart of the Nuclides* (Jpn. Nucl. Data Center, JAERI, 1988).

44. M. Wakasugi, T. Horiguchi, W.G. Jin, Y. Watanabe and Y. Yoshizawa: J. Phys. **B23** (1990) 2173.

45. P.L. Lee and F. Boehm: Phys. Rev. **C8** (1973) 819.

46. R. Engfer, H. Schneuwly, J.L. Vuilleumier, H.K. Walter and A. Zehnder: At. Data. Nucl. Data Tables **14** (1974) 509.

47. S. Raman, C.H. Malarkey, W.T. Milner, C.W. Nestor, Jr. and P.H. Stelson: At. Data Nucl. Data Tables **36** (1987) 1.

48. J.-R. Kropp, H.-D. Kronfeldt and R. Winkler: Z. Phys. **A321** (1985) 57.

49. P. Aufmuth, K. Heilig and A. Steudel: At. Data Nucl. Data Tables **37** (1987) 455.

50. S. Nir: J. Opt. Soc. Am. **60** (1970) 354.

51. Th.A.M.van Kleef, J. Blaise and J.F. Wyart: J. Phys.(Paris) **32** (1971) 609.

52. J. Blaise, Th.A.M.van Kleef and W.F. Wyart: J. Phys.(Paris) **32** (1971) 617.

53. G. Saawatzky and R. Winkler: Z. Phys. **D14** (1989) 9.